AGU PUBLICATIONS

Water Resources Research

RESEARCH ARTICLE
10.1002/2014WR015251

Mathematical analysis of the Saint-Venant-Hirano model for mixed-sediment morphodynamics

G. Stecca[1], A. Siviglia[2], and A. Blom[1]

[1]Faculty of Civil Engineering and Geosciences, Delft University of Technology, Delft, Netherlands, [2]Laboratory of Hydraulics, Hydrology and Glaciology VAW, ETH Zurich, Zurich, Switzerland

Key Points:
- We provide a detailed mathematical analysis of the Saint-Venant-Hirano model
- Imbalances of grainsize distribution induce complex bed perturbation patterns
- The developed formulation is easily amenable to numerical treatment

Supporting Information:
- ReadMe
- Mathematical detail of the analysis

Correspondence to:
G. Stecca,
G.Stecca@tudelft.nl

Citation:
Stecca, G., A. Siviglia, and A. Blom (2014), Mathematical analysis of the Saint-Venant-Hirano model for mixed-sediment morphodynamics, *Water Resour. Res.*, *50*, doi:10.1002/2014WR015251.

Received 6 JAN 2014
Accepted 15 AUG 2014
Accepted article online 19 AUG 2014

Abstract Sediment of different size are transported in rivers under the action of flow. The first and still most popular sediment continuity model able to deal with mixed sediment is the so-called active layer model proposed by Hirano (1971, 1972). In this paper, we consider the one-dimensional hydromorphodynamic model given by the Saint-Venant equations for free-surface flow coupled with the active layer model. We perform a mathematical analysis of this model, extending the previous analysis by Ribberink (1987), including full unsteadiness and grainsize selectivity of the transported load by explicitly considering multiple sediment fractions. The presence of multiple fractions gives rise to distinct waves traveling in the downstream direction, for which we provide an analytical approximation of propagation velocity under any Froude regime. We finally investigate the role of different waves in advecting morphodynamic changes through the domain. To this aim, we implement an analytical linearized solver to analyze the propagation of small-amplitude perturbations of the bed elevation and grainsize distribution of the active layer as described by the system of governing equations. We find that initial gradients in the grainsize distribution of the active layer are able to trigger significant bed variations, which propagate in the downstream direction at faster pace than the "bed" wave arising from the unisize-sediment Saint-Venant-Exner model. We also verify that multiple "sorting" waves carry multiple associated bed perturbations, traveling at different speeds.

1. Introduction

River beds are usually characterized by the presence of mixed sediment. The grainsize distribution can be unimodal and well sorted, as in the case of most sand-bed rivers, or poorly sorted showing varying degrees of bimodality as in the case of most gravel bed rivers [*Parker*, 2004].

The mathematical description of mixed-sediment morphodynamics requires a proper sediment continuity model, relating bed load transport to the size of sediments available at the bed surface and keeping track of the development of stratigraphy. *Hirano* [1971, 1972] was the first to develop such a model. He discretized the bed material using a finite number of classes characterized by a unique grainsize value and put forward the concept of exchange layer (active layer in the English literature), i.e., a fully mixed layer located just under the bed surface. The active layer represents the volume of sediment that interacts with the flow giving rise to bed load fluxes and regulates the exchange with the substrate located underneath.

Despite the more recent introduction of a refined vertical-continuous approach to the modeling of size stratification [e.g., *Parker et al*., 2000; *Blom and Parker*, 2004; *Blom et al*., 2008], the active layer model has been the most popular approach to mixed-sediment morphodynamics over the last four decades: it has been used to study, e.g., static bed armoring [*Ashida and Michiue*, 1971], sediment sorting induced by dunes [*Ribberink*, 1987], sediment sorting in bends [*Parker and Andrews*, 1985], bed load sheets [*Seminara et al*., 1996], river bars [*Lanzoni and Tubino*, 1999], and patterns of longitudinal sorting [*Hoey and Ferguson*, 1994]. More details on its applications are given in *Parker et al*. [2000] and references therein.

To serve different purposes, it has received numerous improvements and modifications by various authors: *Armanini and Di Silvio* [1998], *Parker* [1991], and *Di Silvio* [1992] introduced a term describing the time evolution of the storage of sediment in a thin bed load layer on top of the active layer; *Armanini and Di Silvio* [1998], *Holly and Rahuel* [1990], and *Di Silvio* [1992] developed a formulation for suspended load transport; *Parker* [1991] introduced a formulation for particle abrasion; *Parker* [1991], *Hoey and Ferguson* [1994], and *Toro-Escobar et al*. [1996] modified the formulation for the depositional flux to the substrate; *Ribberink*

[1987] and *Di Silvio* [1992] introduced an additional layer below the active layer to account for vertical sediment exchange due to occasionally deep bed form throughs; *Sieben* [1997] included an adaptation length in the bed load formulation for the stabilization of the model; and *Sloff et al*. [2001] subdivided the substrate into different layers for bookkeeping purposes.

The active layer model is also, by large extent, the most widely used strategy to account for mixed sediment in numerical models: it has been used for studying, e.g., sediment overloading [*Ribberink*, 1987], morphodynamic evolution of mountain streams [*Sieben*, 1997] and sediment pulses in mountain streams [*Cui and Parker*, 2005], downstream fining by selective transport [*Hoey and Ferguson*, 1994], development of size stratification of the bed [*Viparelli et al*., 2010], and pool-riffle dynamics [*Mazza de Almeida and Rodríguez*, 2011] and is implemented in mainstream morphodynamic software, e.g., Delft3D [*Sloff et al*., 2001] and BASEMENT [*Vetsch et al*., 2006–2013].

Yet despite its widespread use, the mathematical behavior of the active layer model has not been completely explored. A fundamental contribution is due to *Ribberink* [1987]. He analyzed the system of governing equations neglecting grainsize selectivity of bed load and assuming quasi-steady flow. He developed approximations to the speed of the "bed wave" and "sorting wave," where the latter is the speed associated with a model for the evolution of the average diameter in the mixture (resembling all the active layer equations) and the former is identical to the celerity of bed perturbations in the uniform-size (unisize)-sediment case [*De Vries*, 1965]. These outcomes have been used to interpret both field data [*Mosselman et al*., 2008] and numerical results [*Sloff and Mosselman*, 2012] in sorting-dominated contexts. An alternative analysis was performed by *Suzuki* [1976], who derived approximations to the characteristic speeds of the system by retaining independent active layer equations. His analysis, still limited by the assumption of quasi-steady flow, identifies distinct "sorting" celerities associated with the distinct active layer equations. More refinements have been put forward by *Sieben* [1997]. He obtained a graphical representation of the characteristic celerities for the unsteady model in a two-fraction setup, developed simplified analytical models under quasi-steady flow approximation and analyzed the features of numerical solutions.

The analysis of *Ribberink* [1987] also addressed in a simplified manner the question whether the model is hyperbolic, i.e., characterized by real characteristic celerities. This is of paramount importance since only hyperbolic models are adequate for representing time-advancing problems [e.g., *Toro*, 2001], which are fully determined by the initial and boundary conditions. Otherwise, if the wave speeds are complex, which may happen for the Saint-Venant-Hirano model when the active layer degrades into a finer substrate [*Ribberink*, 1987], the problem becomes elliptic. Elliptic problems require boundary conditions to be set over the entire boundary for all the independent variables. This is acceptable for steady problems, where all independent variables are spatial coordinates, but does present a severe conceptual problem if one of the independent variables is time, as in the present case. Here the required condition at the upper time boundary implies the present to depend on the future, which is physically nonsensical [*Mosselman*, 2012]. Thus, the Hirano model in the elliptic range is unsuitable for morphodynamic predictions [*Ribberink*, 1987; *Sieben*, 1997].

In the present paper, we aim at performing a more complete mathematical analysis of the Hirano active layer model coupled with the unsteady Saint-Venant equations for one-dimensional free-surface flow. After rewriting the problem in matrix-vector form, we will develop approximations to all the system eigenvalues, which provide the speeds of the small-amplitude waves described by the model, and we will determine its hyperbolicity domain.

Our analysis extends the available wave speed estimates by *Ribberink* [1987] by considering all the "sorting" characteristic directions associated with each individual active layer equation, i.e., avoiding reduction of the active layer model to a single equation for the average diameter. Here, by "sorting" characteristic directions we mean those directions along which most of the changes in the grainsize distribution of the active layer are advected. Our approach enables us to develop approximations to all the wave speeds in the system under high-transport conditions, and to show that, if grainsize selectivity is considered, the "sorting" waves propagate at different speeds. Furthermore, it allows us to consider low and partial transport conditions, in which only some fractions are transported by the flow.

Finally, we consider the role of each wave in propagating morphodynamic changes. In this respect, we show that each "sorting" wave issuing from an infinitesimal localized perturbation in the grainsize distribution of the active layer also carries significant changes in the bed profile, due to the associated bed load gradients.

The paper proceeds as follows. In section 2, we set the coupled Saint-Venant-Hirano model and rewrite it in matrix-vector form. In section 3, we analyze its eigenstructure in order to develop analytical approximations for its eigenvalues and to determine the hyperbolicity domain, and numerically test these achievements. In section 4, we develop an analytical solver for the linearized problem and apply it to study the wave dynamics driven by the mixed-sediment model. Finally, in section 5, we discuss the validity of our assumptions and some implications of our analysis, and conclusions are drawn in section 6.

2. The Mathematical Model

We consider a one-dimensional hydrostatic model, which describes unsteady free-surface flow over a cohesionless bottom composed of mixed sediment. Friction exerted by flow over sediment induces sediment transport, which is assumed to occur only as bed load. The active layer approach of *Hirano* [1971, 1972] is employed in order to allow for changes in the grainsize distribution of the bed surface and to account for the development of size stratification. The resulting mathematical model is composed of a set of governing equations expressing physical principles (conservation of water and sediment mass and the momentum principle) and by closure relations for friction and sediment transport.

2.1. System of Governing Equations

The one-dimensional, nonlinear system of partial differential equations (PDEs) considered in this paper includes equations for conservation of water mass (the continuity equation),

$$\frac{\partial h}{\partial t}+\frac{\partial q}{\partial x}=0\,, \tag{1}$$

for the momentum principle for the water phase,

$$\frac{\partial q}{\partial t}+\frac{\partial}{\partial x}\left(\frac{q^2}{h}+\frac{1}{2}gh^2\right)+gh\frac{\partial \eta}{\partial x}=-ghS_f\,, \tag{2}$$

and for the conservation of sediment mass (the Exner equation):

$$\frac{\partial \eta}{\partial t}+\frac{\partial q_b}{\partial x}=0\,. \tag{3}$$

In (1)–(3), $h(x,t)$[m] denotes flow depth, $q(x,t)$ [m^2s^{-1}] flow discharge per unit width, $g=9.81$ ms^{-2} is the acceleration due to gravity, $\eta(x,t)$ [m] is bed elevation, $S_f(x,t)$ is the dimensionless friction slope, and $q_b(x,t)$ [m^2s^{-1}] represents total sediment discharge per unit width multiplied by the factor $1/(1-p)$, where p is bed porosity. We furthermore define water velocity as $u(x,t)=q/h$ [ms^{-1}]. Equations (1)–(3) constitute the Saint-Venant-Exner model, describing one-dimensional morphodynamics under the assumption of unisize sediment, i.e., if only one representative sediment diameter is considered.

To deal with mixed sediment, we adopt (i) a representation of the sediment mixture using discrete fractions, (ii) a vertical discretization of the river bed, in order to keep track of size stratification, and (iii) a grainsize-specific sediment continuity model.

The sediment mixture is discretized using N fractions, each one characterized by one representative grain diameter d_{sk}, where k is an index spanning the range from 1 to N. The sediment discharge of each size fraction q_{bk} is defined using appropriate closure relations, which will be described in section 2.2. The total sediment discharge q_b to be used in (3) is then given by

$$q_b=\sum_{k=1}^{N} q_{bk}\,. \tag{4}$$

For vertical discretization of river bed size stratification, following *Hirano* [1971] and *Parker* [1991, 2004], we consider two layers (see Figure 1). The *active layer* is a moving volume, having thickness L_a [m], located immediately under the bed surface. Though L_a can in principle vary with space and time, in this paper we restrict our attention to constant active layer thickness. Thus, the vertical displacement of the active layer varies with the bed elevation $\eta(x,t)$. Below the active layer, the *substrate* is found, and the interface between the active layer and the substrate is located at elevation $z=\eta-L_a$ (see Figure 1). The active layer is

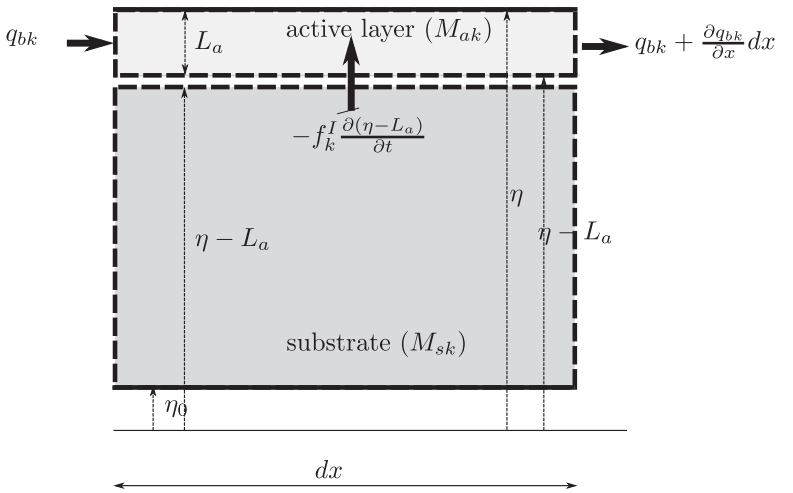

Figure 1. Sketch and notation of the vertical discretization of the river bed and sediment fluxes.

assumed to be vertically mixed [*Hirano*, 1971] and the vertically averaged volume fraction content of size fraction k is denoted with $F_{ak}(x,t)$. The substrate, instead, is not vertically mixed and its fraction content is denoted with $f_{sk}(x,z,t)$.

The active layer provides a source of sediment to be entrained into the flow, giving rise to sediment discharge q_{bk}. The grainsize distribution of the active layer F_{ak} is assumed to be representative of that of the bed surface in the evaluation of bed load, as we shall see in section 2.2. The substrate layer instead does not contribute to bed load discharge. Exchange of sediment between the two layers occurs only by net aggradation and degradation of the interface at $z=\eta-L_a$. This results in a vertical flux of sediment mass, which is compensated by consumption or creation of new substrate on top of the layer.

The following constraints over the sediment fraction values hold

$$0 \leq F_{ak} \leq 1\,, \quad 0 \leq f_{sk} \leq 1 \qquad \text{for } 1 \leq k \leq N \tag{5}$$

and

$$\sum_{k=1}^{N} F_{ak} = 1\,, \qquad \sum_{k=1}^{N} f_{sk} = 1\,. \tag{6}$$

For each size fraction, we define two sets of conserved variables, i.e., variables for which physically meaningful balance laws can be established [see e.g., *Toro*, 2009]. They are

$$M_{ak} = F_{ak} L_a\,, \quad M_{sk} = \int_{\eta_0}^{\eta - L_a} f_{sk}(z)\mathrm{d}z\,, \tag{7}$$

where η_0 is a constant reference elevation datum well embedded in the substrate (see Figure 1). M_{ak} and M_{sk} have the dimension of lengths ([m]) and represent the sediment mass of the kth fraction per surface area in the active and substrate layer, divided by the constant sediment density, in the active and substrate layer. For this reason, M_{ak} and M_{sk} will be termed sediment mass variables.

The constraint (6) can be rewritten as

$$\sum_{k=1}^{N} M_{ak} = L_a\,, \quad \sum_{k=1}^{N} M_{sk} = \eta - L_a - \eta_0\,. \tag{8}$$

Finally, the required grainsize-specific continuity model is defined imposing the mass conservation principle in the active layer,

$$\frac{\partial M_{ak}}{\partial t} = -f_k^I \frac{\partial}{\partial t}(\eta - L_a) - \frac{\partial q_{bk}}{\partial x}\,, \tag{9}$$

and in the substrate

$$\frac{\partial M_{sk}}{\partial t} = f_k^l \frac{\partial}{\partial t}(\eta - L_a)\,. \tag{10}$$

In (9) and (10), $f_k^l(x,t)$ denotes the volume fraction content at the interface between the active and substrate layer. Since at that location a discontinuity in fraction content is allowed, following *Hirano* [1971] and *Ribberink* [1987] its value at the interface is evaluated as

$$f_k^l = \begin{cases} F_{ak} & \text{if } \dfrac{\partial}{\partial t}(\eta - L_a) > 0 \\ f_{sk}(z = \eta - L_a) & \text{if } \dfrac{\partial}{\partial t}(\eta - L_a) < 0 \end{cases}. \tag{11}$$

Equation (11) states that the fraction content at the active-substrate interface to be used in (9) and (10) is equal to that of the active layer in case of aggradation of the active-substrate layer interface and to that of the top of the substrate layer otherwise. Alternative relations (not used in this paper) have been proposed by *Parker* [1991], *Hoey and Ferguson* [1994], and *Toro-Escobar et al.* [1996]. By the definition (11) and the constraint (5), the interface fraction content is subject to the constraint

$$0 \le f_k^l \le 1 \qquad \text{for } 1 \le k \le N\,. \tag{12}$$

The final form of equations (9) and (10) is found using the Exner equation (3) to evaluate the term $\partial\eta/\partial t$ and considering temporal constancy of the active layer thickness, i.e.

$$\frac{\partial L_a}{\partial t} = 0\,. \tag{13}$$

We obtain the following active layer conservation equations:

$$\frac{\partial M_{ak}}{\partial t} + \frac{\partial q_{bk}}{\partial x} - f_k^l \frac{\partial q_b}{\partial x} = 0 \tag{14}$$

and substrate layer conservation equations:

$$\frac{\partial M_{sk}}{\partial t} + f_k^l \frac{\partial q_b}{\partial x} = 0\,. \tag{15}$$

Notice that by constraints (8) and the assumption (13), only $N-1$ independent active layer and substrate layer equations can be set.

In summary, the coupled Saint-Venant-Hirano model is finally given by $2N+1$ PDEs, namely

1. the Saint-Venant-Exner equations (1)–(3) (3 PDEs) and

2. the active and substrate layer mass conservation equations (14) and (15) ($2(N-1)$ PDEs)

and by the definition (4) and constraints (8). It is worth mentioning that the model automatically reduces to the Saint-Venant-Exner model (1)–(3) for unisize sediment if only one sediment fraction is considered.

2.2. Closure Relations

Closure relations are required for the evaluation of the friction slope S_f in the momentum equation (2) and bed load transport of each fraction in equations (14) and (15). The bed load transport of each fraction is also required for the evaluation of total bed load flux (4), to be used in (3), (14), and (15).

The theoretical analysis in this paper focuses on the propagation of small-amplitude waves. These waves are the fastest carriers of information described by the model and propagate hydromorphodynamic changes along the characteristic directions over short temporal and spatial scales. In this case, the effect of friction in the momentum equation is commonly assumed to be negligible, see e.g., *Lyn* [1987] and *Lyn and Altinakar* [2002] for the unisize-sediment case and *Ribberink* [1987] for the present mixed-sediment case. Thus, throughout the paper we set $S_f = 0$ in equation (2), and this assumption is discussed in section 5.

The sediment discharge q_{bk} of each fraction is given by

$$q_{bk} = F_{ak} Q_{bk} = \frac{M_{ak}}{L_a} Q_{bk} \,, \tag{16}$$

where Q_{bk} is the transport capacity for the case that the bed would consist only of the size fraction k (in the following, simply termed as the transport capacity of fraction k). Q_{bk} shall be evaluated using a bed load transport relation, as function of the local hydrodynamic conditions.

Ribberink [1987] neglected grainsize selectivity of bed load in his characteristic analysis of the Saint-Venant-Hirano model (chapter 5.1.1 in the thesis), that is, all the classes are characterized by the same transport capacity. This idealized assumption can be acceptable only when sediment transport is very intense but is far away from standard and realistic conditions in rivers. A distinctive feature of the analysis in this paper is the assumption of grainsize selectivity. The present analytical framework can accommodate any bed load relation able to account for grainsize selectivity, e.g., those of *Ashida and Michiue* [1972], *Parker* [1990], or *Wilcock and Crowe* [2003]. Among them, we use the bed load transport relation of *Meyer-Peter and Müller* [1948] in conjunction with the hiding-exposure correction of *Egiazaroff* [1965], which reads

$$Q_{bk} = \text{sign}\,(q)\, A \frac{\sqrt{g \Delta d_{sk}^3}}{1-p} \max\left((\theta_k - \xi_k \theta_c), 0\right)^B \,, \tag{17}$$

where p (constant) is the bed porosity, A and B are dimensionless constant parameters, and θ_c is the critical Shields stress. Throughout this paper, we use $p = 0.4$, $A = 8$, $B = 3/2$, and $\theta_c = 0.047$. Furthermore, we define $\Delta = \rho_s/\rho - 1$, where $\rho_s = 2650\ \text{kg m}^{-3}$ and $\rho = 1000\ \text{kg m}^{-3}$ are sediment and water density. θ_k is the Shields stress relative to the kth sediment fraction, defined as

$$\theta_k = \frac{q^2}{\Delta d_{sk} C^2 g h^2} \,, \tag{18}$$

where C is the dimensionless Chézy coefficient, here assumed as constant. Finally in (17), ξ_k is the hiding factor for the kth fraction, which reads

$$\xi_k = \left(\frac{\log_{10} 19}{\log_{10}\left(19 \frac{d_{sk}}{\overline{d_s}}\right)} \right)^2 \,, \tag{19}$$

where $\overline{d_s} = \sum_{k=1}^{N} F_{ak} d_{sk}$ is the mean sediment diameter in the active layer. The hiding factor reduces the mobility of fine grains in the mixture compared to the unisize-sediment case and increases that of coarse grains, thus promoting conditions closer to equal mobility with respect to the case without hiding correction ($\xi_k = 1$). In other words, the hiding-exposure correction reduces the grainsize selectivity of the transport process, but in our case not to the extent that grainsize selectivity is fully neglected. We emphasize since now that considering the hiding correction in the form (19), or in a different form, e.g., in the power law form set by *Parker* [1990], or simply neglecting it, does not have significant impact over our eigenstructure analysis, since it only affects the values of transport capacity and threshold of motion, but not our conclusions on the wave celerities under different transport regimes, on the physical role of waves, on hyperbolicity of the mathematical model.

2.3. The System in Matrix-Vector Form

The system given by (1–3), (14), and (15), assuming $S_f = 0$, can be recast in matrix-vector form as

$$\frac{\partial \mathbf{Q}}{\partial t} + \mathbf{A} \frac{\partial \mathbf{Q}}{\partial t} = \mathbf{0} \,, \tag{20}$$

with

$$\mathbf{Q} = \left[h,\ q,\ \eta,\ \underbrace{M_{a1},\ \ldots,\ M_{aN-1}}_{N-1},\ \underbrace{M_{s1},\ \ldots,\ M_{sN-1}}_{N-1} \right]^T \,, \tag{21}$$

and

$$\mathbf{A}=\left[\begin{array}{ccc|c|c}
0 & 1 & 0 & [0] & [0] \\
gh-u^2 & 2u & gh & [0] & [0] \\
\dfrac{\partial q_b}{\partial h} & \dfrac{\partial q_b}{\partial q} & 0 & \left[\dfrac{\partial q_b}{\partial M_{al}}\right] & [0] \\
\hline
\left[\dfrac{\partial q_{bk}}{\partial h}-f_k^l\dfrac{\partial q_b}{\partial h}\right] & \left[\dfrac{\partial q_{bk}}{\partial q}-f_k^l\dfrac{\partial q_b}{\partial q}\right] & [0] & \left[\dfrac{\partial q_{bk}}{\partial M_{al}}-f_k^l\dfrac{\partial q_b}{\partial M_{al}}\right] & [0] \\
\hline
\underbrace{\left[f_k^l\dfrac{\partial q_b}{\partial h}\right]}_{1} & \underbrace{\left[f_k^l\dfrac{\partial q_b}{\partial q}\right]}_{1} & \underbrace{[0]}_{1} & \underbrace{\left[f_k^l\dfrac{\partial q_b}{\partial M_{al}}\right]}_{N-1} & \underbrace{[0]}_{N-1}
\end{array}\right]\begin{array}{l}\}1\\ \}1\\ \}1\\ \}N-1\\ \}N-1\end{array} \tag{22}$$

In (21) and (22), $\mathbf{Q}$ has size $(2N+1)\times 1$ and $\mathbf{A}$ has size $(2N+1)\times(2N+1)$. In order to accommodate an arbitrary number $N-1$ of active and substrate layer equations, the matrix $\mathbf{A}$ is here defined by blocks, whose size is indicated at its bottom and right. The integer indices k and l span the range between 1 and $N-1$ and identify the column and row numbering within these blocks, respectively. The matrix includes as 3×3 upper-left block the system matrix of the Saint Venant-Exner model for unisize sediment and reduces to that if one single sediment class ($N=1$) is considered. For the sake of clarity, the matrix is rewritten in extended form in Appendix A.

3. Mathematical Analysis

In this section we will analyze the eigenstructure of the system matrix (22). In detail, we will provide approximations to the system eigenvalues, which yield the celerities of small-amplitude perturbations as described by the model, and provide an interpretation of the role of these waves in propagating hydrodynamic and morphodynamic changes. We will also determine under which physical conditions these eigenvalues are complex, denoting loss of hyperbolic behavior of the model. These results will be tested numerically.

3.1. Preliminaries

We aim at rewriting the system matrix (22) into a more compact form for subsequent analysis, highlighting the dependences on physically meaningful parameters. We introduce

$$F_r=\frac{q}{\sqrt{gh^3}}\,,\quad \psi=\frac{\partial q_b}{\partial q}\,, \tag{23}$$

where F_r is the Froude number and ψ represents the variation in total bed load discharge per unit variation in water discharge. The latter parameter, already used by several authors, e.g., *De Vries* [1965] and *Lyn and Altinakar* [2002], represents a measure of the intensity of total bed load in the flow.

We observe that the last $N-1$ rows in $\mathbf{A}$ (22), which correspond to the substrate layer equations (15), are linearly dependent on the third row resembling the Exner equation (3), since they contain the same entries multiplied by the scalar f_k^l, and that the last $N-1$ columns are null. Therefore, $N-1$ of the eigenvalues $\mathbf{A}$ are readily found to be identically equal to zero. In the following analysis, for the sake of simplicity, the corresponding lines and columns will be discarded, without altering the remaining eigenvalues. We will thus consider the reduced matrix which only contains the upper 3×3 Saint-Venant-Exner block and the $N-1$ additional rows and columns of the active layer equations. After some algebraic manipulations, which are presented in detail in the supporting information to this article, the reduced matrix is written as

$$\mathbf{A}_r=\left[\begin{array}{ccc|c}
0 & 1 & 0 & [0] \\
u^2\left(\dfrac{1}{F_r^2}-1\right) & 2u & \dfrac{u^2}{F_r^2} & [0] \\
-u\psi & \psi & 0 & \left[\dfrac{Q_{bl}-Q_{bN}}{L_a}\right] \\
\hline
\underbrace{[-u\gamma_k\psi]}_{1} & \underbrace{[\gamma_k\psi]}_{1} & \underbrace{[0]}_{1} & \underbrace{\left[\delta_{k,l}\dfrac{Q_{bl}}{L_a}-f_k^l\dfrac{Q_{bl}-Q_{bN}}{L_a}\right]}_{N-1}
\end{array}\right]\begin{array}{l}\}1\\ \}1\\ \}1\\ \}N-1\end{array}\,, \tag{24}$$

where $\delta_{k,l}$ is the Kronecker delta function, taking the value of 1 if $k = l$ and 0 otherwise. In (23), the dimensionless parameter

$$\gamma_k = c_k - f_k^l \tag{25}$$

is defined as the difference between the grainsize distribution

$$c_k = \frac{1}{\psi}\frac{\partial q_{bk}}{\partial q} = \frac{\partial q_{bk}/\partial q}{\partial q_b/\partial q} \tag{26}$$

and the grainsize distribution measured at the interface between the active and substrate layer f_k^l. In (26), the term $\partial q_{bk}/\partial q$ represents the variation of bed load discharge of the kth fraction for a unit variation of water discharge. Hence, with the definition of ψ (23), c_k represents the increase in the transport of the kth fraction relative to the increase of total bed load, with increasing water discharge. By the definitions (25), (23), and (4) and the condition (12), the constraint

$$-1 \le \gamma_k \le 1 \qquad \text{for } 1 \le k \le N \tag{27}$$

holds.

While specifying the diameter of each class, we stipulate that sediment fractions are ordered by increasing diameter, i.e.

$$d_{sk} < d_{sk+1} \qquad \text{for } 1 \le k \le N-1\,, \tag{28}$$

which gives rise to decreasing transport capacities, i.e., $|Q_{bk}| \ge |Q_{bk+1}|$, as predicted by the bed load relation (17).

It can be proven that the third line in $\mathbf{A}_r$ (23) resembling the Exner equation (3) and the $N-1$ lines located underneath, which arise from the active layer equation (14), are linearly independent, provided the transport capacity of each fraction, predicted by (17), is nonzero. The system eigenstructure is thus markedly dependent on the considered transport regime. For transport rates from moderate to high, when all the fractions are mobile, $N-1$ independent active layer equations are retained and $N-1$ waves having nonzero celerity will arise from them. This case is analyzed in section 3.2. Conversely, under partial transport conditions, when only P sediment fractions are mobile, with $1 \le P < N$, a number $N-P$ of linearly dependent active layer equations will be found, which will produce a corresponding number of waves having null celerity, as we shall see in section 3.6.

Finally, for the subsequent hyperbolicity analysis in section 3.3, we specify the matrix for the particular case of a two-fraction mixture, which reads

$$\mathbf{A}_r = \begin{bmatrix} 0 & 1 & 0 & 0 \\ u^2\left(\frac{1}{F_r^2}-1\right) & 2u & \frac{u^2}{F_r^2} & 0 \\ -u\psi & \psi & 0 & \frac{Q_{b1}-Q_{b2}}{L_a} \\ -u\gamma_1\psi & \gamma_1\psi & 0 & \frac{(1-f_1^l)Q_{b1}+f_1^l Q_{b2}}{L_a} \end{bmatrix}, \tag{29}$$

with

$$\gamma_1 = c_1 - f_1^l \tag{30}$$

and

$$c_1 = \frac{1}{\psi}\frac{\partial q_{b1}}{\partial q} = \frac{\partial q_{b1}/\partial q}{\partial q_b/\partial q}\,. \tag{31}$$

c_1 (31) represents the increase in the transport of fine material (fraction 1) relative to the increase of total bed load, with increasing water discharge. Thus, γ_1 (30) is positive if c_1 (31) is higher than the content f_1^l of fine material in the mixture found at the active layer-substrate interface, and it is negative otherwise. As we show in the supporting information, c_1 is always higher than the content of the first fraction in the active

layer F_{a1}, provided a grainsize-selective bed load relation such as (17) is used. From this observation, it follows that, by assuming grainsize selectivity and considering two mobile fractions, only the case $\gamma_1 > 0$ is allowed under aggradational conditions, i.e., when f_1^I (11) is equal to F_{a1}, and that the case $\gamma_1 < 0$ can only occur in case of degradation into a substrate which has finer grainsize distribution than that given by c_1 (31). Under partial transport conditions instead, when the second fraction is immobile, the case $\gamma_1 \geq 0$ is always found both under aggradational and degradational conditions, since in that case c_1 (31) is found to be identically equal to 1.

3.2. High Sediment Transport: Analytical Eigenvalue Approximations

In this section, we derive analytical approximations for the eigenvalues of the system matrix (23) written for an arbitrary number N of sediment fractions. These eigenvalues provide the speeds of small-amplitude waves as described by the system of governing equations, under the assumption that all fractions are transported by the flow giving rise to relatively high total sediment discharge. Initially in this section, we will make the hypothesis that these eigenvalues are real, i.e., that the system is hyperbolic; the conditions for hyperbolicity will be discussed in the next section.

The unisize-sediment case ($N = 1$), in which the model reduces to the Saint-Venant-Exner model, has been thoroughly analyzed by *De Vries* [1965], *Lyn* [1987], *Lyn and Altinakar* [2002], and *Lanzoni et al*. [2006]. In particular, *Lyn* [1987] and *Lyn and Altinakar* [2002] use a first-order perturbation approach in terms of the small parameter ψ (23), which in alluvial rivers typically has magnitude $\mathcal{O}(10^{-2})$ or lower [*Lyn*, 1987; *Lanzoni et al*., 2006]. Their approximations to the system eigenvalues have the form

$$\lambda_{1,2}^* = 1 \pm \frac{1}{F_r}, \quad \lambda_3^* = \frac{\psi}{1-F_r^2}, \tag{32}$$

where $\lambda_i^* = \lambda_i / u$ ($i = 1, 2, 3$) are the dimensionless eigenvalues. This approximation is valid under well-developed sub or supercritical regime, under the condition $|1-F_r^2| > \mathcal{O}(\sqrt{\psi})$, in practice, in the ranges $F_r < 0.8$ and $F_r > 1.2$. Physically, the characteristic speed λ_3^* (32) has been identified as the celerity of bed perturbations in the quasi-steady analysis of *De Vries* [1965]. Thus, from now on, we will term this celerity and the associated wave as the "bed" celerity and "bed" wave. The "bed" wave travels in the downstream direction under (well-developed) subcritical flow, when its celerity is positive, and propagates in the upstream direction under supercritical flow [e.g., *Lyn and Altinakar*, 2002]. The speeds $\lambda_{1,2}^*$, which are equal to those of the fixed-bed shallow water model, identify the celerity of waves mainly carrying perturbations of the flow variables [*Lyn and Altinakar*, 2002].

Close to critical conditions, i.e., for $|1-F_r^2| < \mathcal{O}(\sqrt{\psi})$ (roughly for $0.8 < F_r < 1.2$), the quasi-steady flow approximation is not valid since λ_3^* in (32) tends to infinity. In this case, a different perturbation approach [*Lyn*, 1987; *Lyn and Altinakar*, 2002] yields

$$\lambda_{1,2}^* = \frac{1}{4}\left(1 - \frac{1}{F_r^2}\right) \pm \frac{1}{4}\sqrt{\left(1 - \frac{1}{F_r^2}\right)^2 + \frac{8\psi}{F_r^2}}, \quad \lambda_3^* = \frac{3}{2} + \frac{1}{2F_r^2}. \tag{33}$$

Lyn and Altinakar [2002] show that under transcritical conditions both of the waves having celerity $\lambda_{1,2}^*$ (33) convey most of perturbations in bed elevation in the upstream and downstream direction simultaneously, while the fast downstream-traveling wave λ_3^* is essentially a hydrodynamic wave.

Let us now consider the multiple-fraction case. *Ribberink* [1987] performed a characteristic analysis of the system under the following simplifying assumptions:

1. use of a simplified sorting model, resembling all the active layer equations in one equation for the average diameter $\overline{d_s} = \sum_{k=1}^{N} F_{ak} d_{sk}$;
2. quasi-steady flow: only the Exner equation (3) and the equation for $\overline{d_s}$ are considered;
3. that the total sediment discharge depends only on water velocity and mean sediment diameter; and
4. that in aggradational conditions ($\partial(\eta - L_a)/\partial t > 0$), the grainsize distribution of bed load is equal to that at the interface between the active layer and the substrate.

It is worth noticing that the last hypothesis implies that grainsize selectivity is neglected. Under aggradational conditions ($\partial_t(\eta - L_a) > 0$), the analysis yields two real characteristic celerities

$$\lambda_3^* = \frac{\psi}{1-F_r^2}, \quad \lambda_4^* = \frac{q_b}{uL_a}. \tag{34}$$

Here λ_3^* is identical to λ_3^* in (32) and has the same physical meaning, while λ_4^* represents the propagation celerity of perturbations in the average diameter of the mixture, associated with changes in the grainsize distribution in the active layer. We term it hereinafter as the celerity of the "sorting" wave. A more refined expression for the "sorting" celerity is derived by *Mosselman et al*. [2008], taking also into account the difference in the mean diameter between the bed load and the active layer material.

In (34), λ_4^* is positive for any Froude and its magnitude is proportional to the inverse of active layer thickness: a thinner active layer gives rise to higher values of the eigenvalues and then faster "sorting" wave propagation. The ratio λ_4^*/λ_3^* is found to be in the range $0.3 \div 4$ [*Ribberink*, 1987] or $2 \div 8$ [*Sloff and Mosselman*, 2012]. This implies that the "sorting" wave is at least as fast as the "bed" wave and possibly several times faster. However, a limit to the minimum active layer thickness must be set based on the celerity λ_4^*, since it would be unreasonable for the "sorting" wave to travel faster than perturbations in the flow variables [*Sieben*, 1997].

The solution (34) and its variation [*Mosselman et al*., 2008] have the following three limitations:

1. due to the quasi-steady flow assumption, they do not apply to transcritical conditions;
2. they only include a single, representative celerity for the evolution of the average diameter, i.e., λ_4^* in (34), rather than distinct celerities due to various size fractions; and
3. being developed in aggradational conditions, they can be applied to degradation only if the top of the substrate layer has the same grainsize distribution as the active layer, as is done by *Mosselman et al*. [2008].

Suzuki [1976] performed an alternative characteristic analysis of the Saint-Venant-Hirano model, by retaining independent active layer equations for all the fractions. The analysis, which assumes quasi-steady flow and thus applies to well-developed sub or supercritical Froude conditions only, yields distinct "sorting" celerities, having the form

$$\lambda_{3+k}^* = \frac{Q_{bk} + F_{ak}\frac{\partial Q_{bk}}{\partial F_{ak}}}{uL_a} \tag{35}$$

in addition to the three celerities of the unisize-sediment model in (32).

A fully unsteady analysis of the Saint-Venant-Hirano model in the particular case of two sediment fractions was put forward by *Sieben* [1997] under any Froude regime. He found one additional, "sorting" characteristic celerity with respect to those of the unisize-sediment case, which is positive throughout the Froude domain. However, his analysis does not provide a closed-form expression for the characteristic celerities of the Saint-Venant-Hirano model, but only their graphical representation for various values of the active layer thickness.

It is worth pointing out since now that, though in general the "sorting" wave takes a prominent role in propagating changes in the grainsize distribution in the active layer, in principle all the other waves can contribute to streamwise sorting processes, to larger or lower extent. Thus, the name of "sorting" wave shall only serve as a useful, though in principle incorrect, definition. The same considerations hold for the "bed" wave λ_3^* of *De Vries* [1965], which might be not the only wave along which significant bed changes are propagated, especially if sorting processes are considered, as we shall show in section 4. Therefore, while taking advantage of these definitions for rapidly identifying the main physical role of these waves, we will always retain quotation marks.

Next, retaining flow unsteadiness, we will derive an analytical expression for the eigenvalues of the system, written for N fractions. Our analysis still relies on the first-order perturbation approach by *Lyn* [1987] and *Lyn and Altinakar* [2002], where the solution is expanded in terms of the small parameter ψ (23). The present study is restricted to high-transport conditions, in which all the size fractions are mobile and are characterized by transport capacities having similar magnitude. The latter hypothesis, the details of which are explained in the supporting information, still allows the transport capacities of different fractions Q_{bk} to

have distinct (albeit not too different) magnitude, thus allowing for grainsize selectivity, and the case set by *Ribberink* [1987] in which grainsize selectivity is neglected is included as a particular case.

The assumption of transport capacities having similar magnitude allows one to simplify terms $\mathcal{O}(\psi^2)$ or smaller in the characteristic polynomial of $\mathbf{A}_r$ (23), which are not of interest in the present first-order analysis. Then, a first-order perturbation solution in terms of ψ still yields the three eigenvalues of the Saint-Venant-Exner model (32) or (33), which are identical to those found by *Lyn* [1987] in the unisize-sediment case. In addition to them, $N-1$ eigenvalues are found, having the form

$$\lambda^*_{3+k} = \frac{Q_{bk}\left(1-f^l_k\right)+f^l_k Q_{bN}}{uL_a} \qquad \text{for } 1 \le k \le N-1\,. \tag{36}$$

The latter eigenvalues represent the propagation velocity of $N-1$ distinct "sorting" waves as defined above. They are always positive and have magnitude proportional to the inverse of the active layer thickness, like λ^*_4 (34). The full solution is then given by (36) together with the eigenvalues of the Saint-Venant-Exner model (32) or (33) in the relevant Froude regime, thus including $N+2$ eigenvalues, in addition to the $N-1$ null eigenvalues which arise from the substrate conservation equations (see section 3.1). The present approximation improves the estimates (34) in three respects:

1. by inclusion of the fully unsteady Saint-Venant model, it correctly describes all the Froude regimes; thus, the full set of three eigenvalues related to the Saint-Venant-Exner part of the system is explicitly considered;
2. it considers one eigenvalue for each active layer equation, yielding distinct celerities of $N-1$ distinct sorting waves; and
3. it naturally applies also to degradational conditions, provided the problem is hyperbolic (see section 3.5).

In the particular case in which grainsize selectivity is neglected, all the distinct "sorting" eigenvalues in (36) collapse on the "sorting" celerity λ^*_4 (34). This is readily found observing that, if the transport capacities of all fractions Q_{bk} have the same value, Q_{bk} are equal to total bed load q_b by (4), (16), and (6). Our analysis also improves that of *Suzuki* [1976], which yields the eigenvalues approximations (32) and (35), in that it retains flow unsteadiness, thus being able to describe also transcritical conditions.

Finally, we wish to specify the dimensionless parameters which are needed for unique identification of the characteristic celerities. To this aim, the celerities can be given in the self-similar form

$$\lambda^* = \frac{\lambda}{u} = \text{funct}\left(F_r, \psi, d^*_{sk}, L^*_a, F_{ak}, f_{sk}(z=\eta-L_a)\right)\,, \tag{37}$$

provided the constants g, Δ, c_b are defined. In (37), F_r and ψ are given by (23); d^*_{sk} are the dimensionless sediment diameters (one for each sediment fraction); and L^*_a is the dimensionless active layer thickness, which are defined as

$$d^*_{sk} = \frac{d_{sk}}{h}\,, \quad L^*_a = \frac{L_a}{h}\,, \tag{38}$$

where the flow depth h is related to the flow velocity u by the Froude value. To prove that the wave celerities are entirely defined by the dimensionless numbers in the right-hand side of (37), we analyze the dependencies in the entries of the system matrix in the form (23). Here F_r and ψ appear explicitly, and dependence on F_{ak} and $f_{sk}(z=\eta-L_a)$ can be found in f^l_k (11). Moreover, in the ratio

$$\frac{Q_{bk}}{L_a} = u\frac{Q_{bk}}{qL^*_a}\,, \tag{39}$$

which appears in numerous entries of $\mathbf{A}_r$ (23), Q_{bk}/q can be uniquely recovered given d^*_{sk}, F_{ak}, F_r, and ψ, by expressing the Shields stress of each fraction (18) as

$$\theta_k = \frac{F_r^2}{\Delta d^*_{sk} C^2} \tag{40}$$

and setting the dimensionless Chézy coefficient C such that the derivatives of the bed load transport relation (17) return the adopted ψ value (23). Finally, γ_k (25) is also uniquely determined from θ_k (40) and f^l_k.

3.3. Domain of Hyperbolicity

A system of PDEs is hyperbolic if the eigenvalues of the system matrix, describing the propagation speeds of waves carrying variations in variables, are all real. Furthermore, it is said strictly hyperbolic if the eigenvalues are all distinct. In this section, we aim at determining for which values of parameters the Saint-Venant-Hirano model is hyperbolic. This is of paramount importance since only hyperbolic models are adequate for representing time-advancing problems, in which the system evolution is entirely determined by the initial condition and appropriate boundary conditions [e.g., *Toro*, 2001]. Otherwise, if the system eigenvalues are complex, the problem becomes elliptic and requires conditions to be set over the full boundary of the space-time domain, including boundary conditions from future to past. An elliptic model is thus conceptually inadequate for morphodynamic predictions. Furthermore, such change in the mathematical behavior determines marked oscillations in numerical solutions and failure of numerical solvers [*Toro*, 2009; *Sieben*, 1997], as it is has been clearly shown for another system of PDEs by *Castro-Díaz et al*. [2011].

A first analysis of the hyperbolicity domain for the Saint-Venant-Hirano model has been put forward by *Ribberink* [1987], under the simplifying assumptions reported in section 3.2. He found that the model is always hyperbolic under aggradational conditions, while hyperbolicity can be lost when the active layer degrades into a finer substrate, depending on the values of parameters. *Sieben* [1997] identifies one subcase characterized by unconditional ellipticity under degradational conditions which he terms "crossing of eigenvalues." This happens if the "bed" celerity λ_3^* (34) is equal to the "sorting" celerity λ_4^* (34) and the substrate is finer than the active layer.

The present hyperbolicity analysis removes some of the simplifying assumptions made by *Ribberink* [1987]. In particular, here we consider the fully unsteady model, thus including any Froude regime. Moreover, we include grainsize-selective conditions, then extending previous conclusions to sediment transport relations of practical use, e.g., (17). In order to analytically treat the problem, our study is carried out for the two-fraction model (29), for which analytical manipulation is still feasible, using an approach analogous to that presented by *Cordier et al*. [2011]. The present study both applies to the case of two movable fractions, and to the case of partial transport, in which the coarsest fraction (the second fraction) is immobile. In section 3.5, the analysis will be extended to multiple fractions through numerical computation of eigenvalues.

With respect to the γ_1 parameter in (30), we consider the following three cases:

1. $\gamma_1 = 0$. This is typically found in aggradational conditions assuming that the grainsize distribution of the bed load and active layer coincides. It corresponds to the aggradational case without grainsize selectivity considered by *Ribberink* [1987].
2. $\gamma_1 > 0$. Under the assumption that both fractions are mobile, this case is associated with aggradational conditions using grainsize-selective transport relations or to degradation into a coarser substrate. Under the assumption that the second fraction is immobile, this case represents all the aggradational and degradational conditions.
3. $\gamma_1 < 0$. This is found when the active layer degrades into a finer substrate and both fractions are mobile.

By performing the analysis, of which the details are given in the supporting information, we prove the following Propositions:

1. if $\gamma_1 = 0$ the system is always hyperbolic;
2. if $\gamma_1 > 0$ the system is always strictly hyperbolic; and
3. if $\gamma_1 < 0$ hyperbolicity cannot be proven and the system may turn out to be elliptic, depending on the particular values of γ and other parameters. At least one subcase is found for which the system is elliptic for any $\gamma_1 < 0$. This happens if the second-largest wave speed of the Saint-Venant-Exner model $\lambda_{\mathrm{SVE}}^{*(2)}$, which is given by the second-largest eigenvalue in the set (32) or (33) in the relevant Froude regime, has the same magnitude as the "sorting" wave speed approximation (36):

$$\lambda_{\mathrm{SVE}}^{*(2)} = \frac{\left(1-f_1^l\right)Q_{b1}+f_1^l Q_{b2}}{uL_a}\,. \tag{41}$$

The subcase (41) includes the above "crossing of eigenvalues" case found by *Sieben* [1997].

Various strategies to avoid the occurrence of elliptic behavior are documented in the literature. *Ribberink* [1987] developed a three-layer model, in which the presence of an intermediate layer located between the substrate and the active layer smoothens the transition into finer substrate. This strategy reduces but does not fully prevent possible loss of hyperbolicity [*Sieben*, 1997]. *Sieben and Sloff* [1994] tweak the active layer thickness, so as to avoid cases of the type (41). Finally, *Sieben* [1997] developed a stabilization strategy by relaxing the assumption that bed load is in equilibrium with the local transport conditions and thus introducing an adaptation length in the sediment transport formulation.

Apart from these model modifications, possible ellipticity may indicate that the purely advective behavior of the Exner equation (3) and Hirano equations (14) used in conjunction with usual bed load transport relations (17) is too crude an approximation of the physics. Recent theoretical and experimental analysis of sediment transport has shown that the bed load flux also includes a diffusive component [*Ancey and Heyman*, 2014; *Furbish et al*., 2012; *Ballio et al*., 2014]. The findings of *Gray and Ancey* [2011] regarding a model for particle-size segregation in shallow granular avalanches suggest that the ill-posed behavior of the Saint-Venant-Hirano model might be cured by introducing these diffusion terms in the definition of bed load discharge.

3.4. Numerical Verification of Eigenvalue Approximations

In this section, we test our wave speed estimates given by (32), (33), and (36) against the reference solution obtained by numerical computation of the eigenvalues of the system matrix in the form (22).

Results are presented in the dimensionless form (37) as function of the Froude number and keeping the remaining parameters constant. Consistently with the hypotheses upon which the analytical estimates are based, all simulations refer to relatively high total sediment transport, given by $\psi=0.0075$. The dimensionless diameter of all fractions d^*_{sk} is prescribed setting the mean diameter d^*_{sm} and a spread parameter Δ^*_d, in the form

$$d^*_{sk}=d^*_{sm}-\frac{\Delta^*_d}{2}+\frac{\Delta^*_d}{N-1}(k-1)\,. \tag{42}$$

The mean sediment diameter d^*_{sm} (38) and spread parameter Δ^*_d and the dimensionless active layer thickness L^*_a (38) are specified with reference to two sets of real-world cases. The first set refers to the bed form-dominated beds of mild-sloping, lowland rivers (e.g., the Dutch Rhine), for which we consider $d^*_{sm}=0.002$ and $\Delta^*_d=0.002$. For these rivers, the dimensional L_a is usually prescribed as a fraction of dune height, which scales with the flow depth [*Ribberink*, 1987]. Thus, the dimensionless L^*_a will be here assigned as an independent constant, set equal to $L^*_a=0.2$. The second set of simulations refers to plane-bed gravel bed rivers of moderate to high slope, having mean diameter $d^*_{sm}=0.01$ and spread parameter $\Delta^*_d=0.01$. In plane-bed rivers, L_a is usually taken as a multiple of a reference diameter, e.g., $L_a=1.5\div3\,d_{90}$ [*Parker*, 2004]. For the sake of simplicity in the model setup, we here assume $L^*_a=3d^*_{sm}=0.03$. Likewise, L^*_a only depends on the mean diameter.

Results are illustrated in Figures 2 and 3. In both figures, the left side presents bed form-dominated cases under subcritical conditions ($0.2<F_r<0.8$), whereas the right side show plane-bed cases under sub, trans, and supercritical conditions ($0.2<F_r<1.6$). We compare our approximate solution (colored lines) with the reference solution obtained numerically (black, dashed lines). In detail, red lines in our plot indicate the wave speeds related to the Saint-Venant-Exner model (32) and (33) and green lines indicate the "sorting" celerities (36). In bed form-dominated cases, results are complemented by the wave speed estimates (34) by *Ribberink* [1987]. The "bed" and "sorting" wave speeds are depicted by square and circular markers, respectively.

Figure 2 reports the eigenvalues computed in the two-fraction case for aggradational conditions, using the grainsize distribution $F_{a1}=F_{a2}=0.5$ in the active layer. In Figures 2a and 2b, we give an overview of all celerities, while in Figures 2c and 2d we provide zooms to Figures 2a and 2b, respectively, to better observe the behavior of the smallest eigenvalues. Our analytical solution provides an accurate approximation to all eigenvalues. In Figure 2c, our solution is seen to exactly coincide with Ribberink's solution (34), which, however, does not include the largest and smallest eigenvalue in the set, as seen in Figure 2a.

Three of the considered eigenvalues are positive, indicating downstream-propagating waves, and one is negative (upstream-propagating wave). In particular, as shown in Figure 2d, the "sorting" eigenvalue is

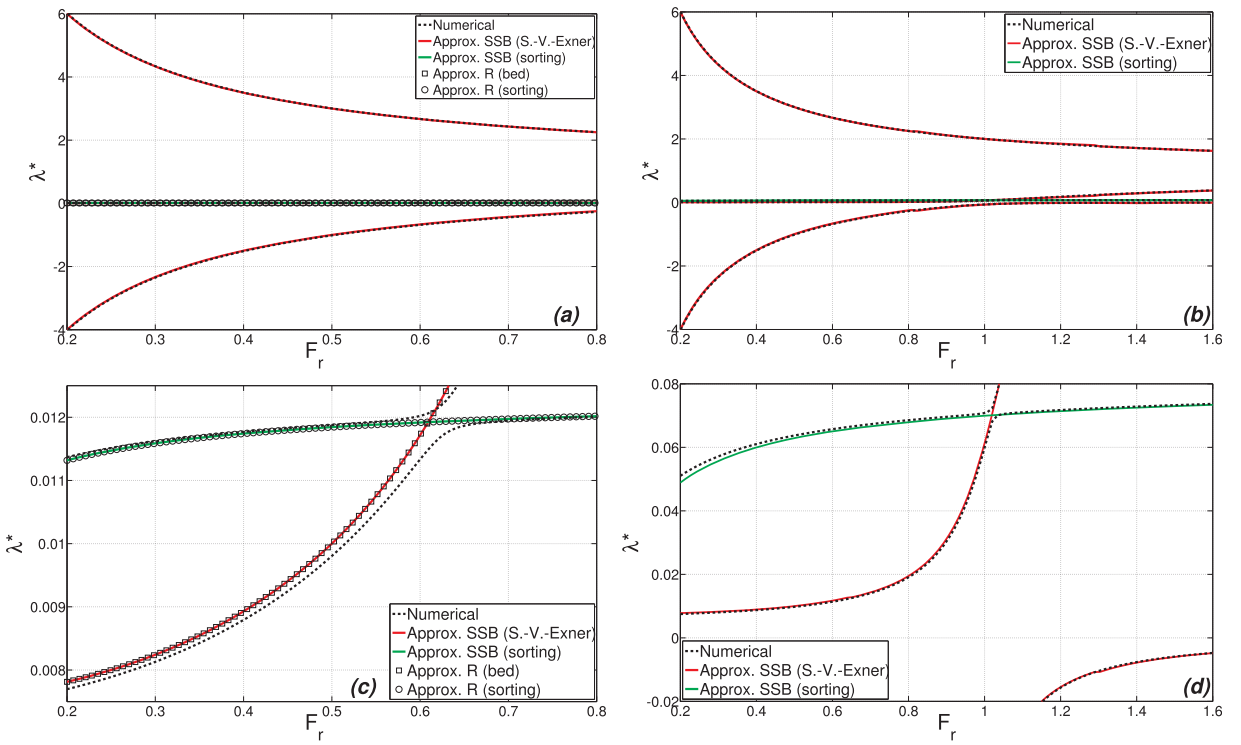

Figure 2. Plot of the system eigenvalues in aggradational conditions as a function of the Froude parameter, under high sediment transport. Our estimates and those due to *Ribberink* [1987] are denoted with SSB and R, respectively. Parameters are $\psi=0.0075$, $N=2$, and $F_{a1}=F_{a2}=0.5$. (a, c) Bed form-dominated cases ($L_a^*=0.2, d_{sm}^*=0.002, \Delta_d^*=0.002$). (b, d) Plane-bed cases ($L_a^*=0.03, d_{sm}^*=0.01, \Delta_d^*=0.01$). Figures 2a and 2b: full plot. Figures 2c and 2d: zoom in correspondence of the slowest waves of the set.

always positive throughout the Froude domain, in agreement with our approximation (36) and with the results obtained by *Sieben* [1997], and weakly dependent of the Froude number.

Moving from the bed form-dominated case in 2(c) ($L_a^*=0.2$ and $d_{sm}^*=0.002$) to the plane-bed case in 2(d) ($L_a^*=0.03$ and $d_{sm}^*=0.01$), the speed of the "sorting" wave is seen to significantly increase with decreasing active layer thickness, in spite of the corresponding increase in sediment diameter of both size fractions. Thus, in a setup typical of plane-bed rivers, the "sorting" waves are expected to travel several times faster than in a bed form-dominated river under the same value of F_r and ψ. In the bed form case of Figure 2c, the "sorting" eigenvalue intersects the second-largest eigenvalue of the Saint-Venant-Exner model, i.e., the "bed" celerity, for $F_r \sim 0.6$. Thus, here for low Froude numbers, the "sorting" wave speed is larger than the bed wave speed, as highlighted by *Sloff and Mosselman* [2012], while this is not true for higher, still subcritical Froude values. In the plane-bed case of Figure 2d, the intersection of the "sorting" eigenvalue and of the second-largest eigenvalue of the Saint-Venant-Exner model is shifted to higher, quasi-critical Froude value as consequence of higher "sorting" wave speed.

In Figure 3, we analyze the eigenvalues obtained under the same parameter setup as in Figure 2, in aggradational conditions, but considering five sediment fractions. We initially focus on Figures 3a–3d, where a rectangular distribution $F_{ak}=0.2$ for all fractions has been set for the active layer. Figures 3a and 3b, reporting the full eigenvalue set, and 3c and 3d, showing zooms of Figures 3a and 3b, respectively, demonstrate overall good agreement between our approximation and the reference numerical solution. The four "sorting" eigenvalues, depicted in green, are weakly dependent of the Froude number. They are all positive and characterized by similar but different magnitude, which is comparable to that of the only "sorting" eigenvalue of the two-fraction case in Figures 2c and 2d. In Figure 3c, it is also worth noticing that the "sorting" wave speed estimate of Ribberink (circles), providing one single characteristic speed related to the evolution of the mean diameter, is incapable of describing the four distinct "sorting" celerities.

In Figures 3e and 3f, we study the sensitivity of eigenvalues to the grainsize distribution of the active layer represented by F_{ak}. Here we impose a very sharp Gaussian grainsize distribution in the active layer, which

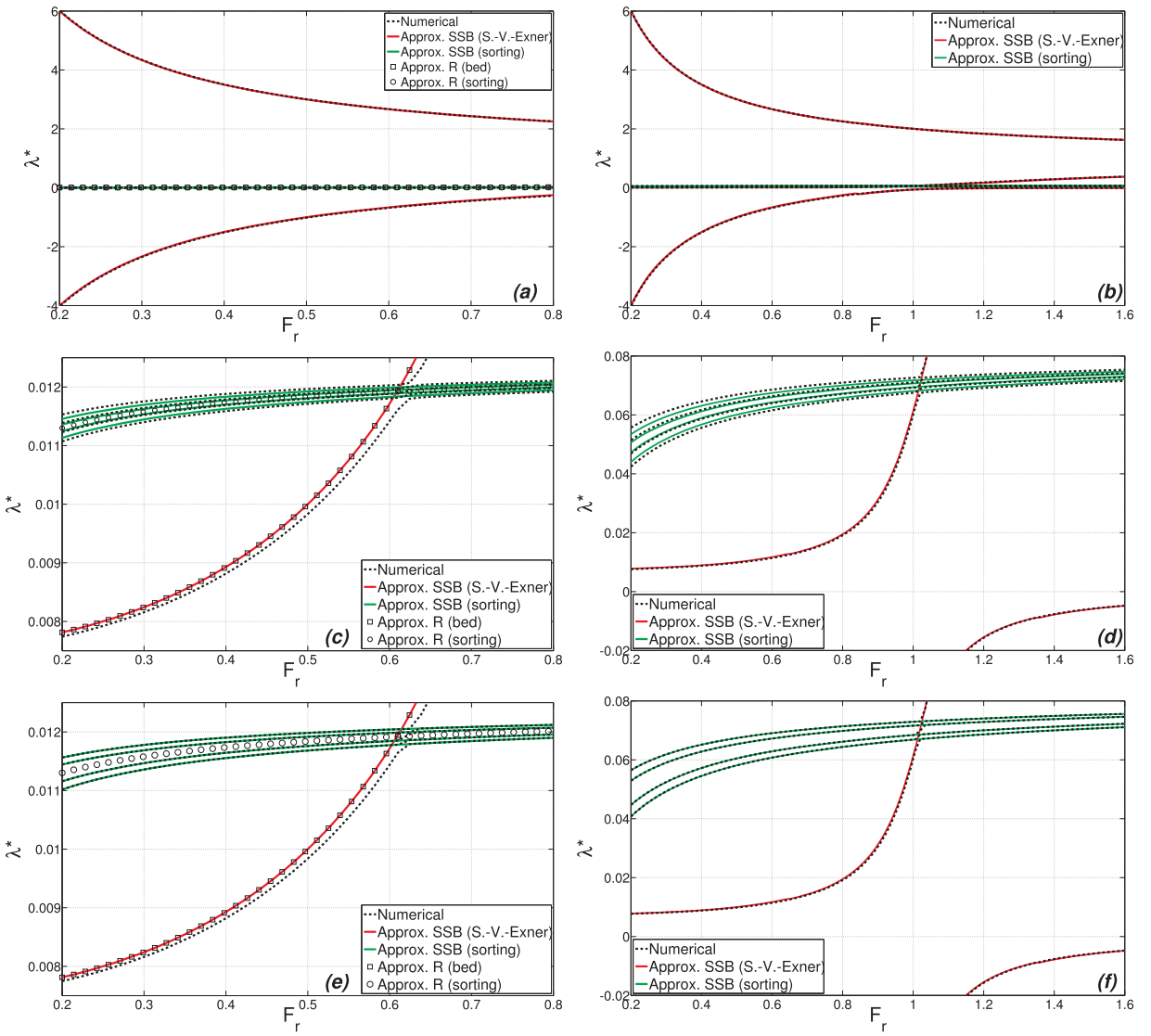

Figure 3. Plot of the system eigenvalues in aggradational conditions as function of the Froude parameter, under high sediment transport. Our estimates and those due to *Ribberink* [1987] are denoted with SSB and R, respectively. $N = 5$ fractions and $\psi = 0.0075$ are considered. (a, c, e) Bed form-dominated cases ($L_a^* = 0.2$, $d_{sm}^* = 0.002$, $\Delta_d^* = 0.002$). (b, d, f) Plane-bed cases ($L_a^* = 0.03$, $d_{sm}^* = 0.01$, $\Delta_d^* = 0.01$). Figures 3a–3d: rectangular distribution of active layer fractions $F_{ak} = 0.2$ for all size fractions. Figures 3c and 3d represent a zoom of Figures 3a and 3b, respectively. Figures 3e and 3f: sharp Gaussian distribution of active layer fractions ($F_{a1} = F_{a5} = 0$, $F_{a2} = F_{a4} = 0.000004$, $F_{a3} = 0.999992$).

gives rise to the discrete values of fractions $F_{a1} = F_{a5} = 0$, $F_{a2} = F_{a4} = 0.000004$, and $F_{a3} = 0.999992$. Comparing Figures 3e and 3f to 3c and 3d, respectively, we observe a very moderate modification in the reference solution, which suggests that the "sorting" wave speeds depend weakly on the grainsize distribution in the active layer. Our estimates (36) turn out to be more accurate in the present case than in that of Figures 3c and 3d.

We have carried out some additional computations (figures not shown here) by neglecting the hiding factor of *Egiazaroff* [1965], i.e., setting $\xi_k = 1$ for all fractions. Apart from a moderate additional spread in the celerity of the "sorting" waves, which can be explained by increased difference between the transport capacities, these results are similar to those in Figure 3, which suggests that the hiding factor does not significantly influence the wave celerities.

3.5. Numerical Study of Hyperbolicity in Degradational Conditions

Here we carry out a numerical study of the hyperbolicity domain in a multiple-fraction setup (five fractions) in degradational conditions to complement our analytical study for two-fraction mixtures in section 3.3. We use a substrate finer than the active layer, which may trigger elliptic behavior for some parameter values. In

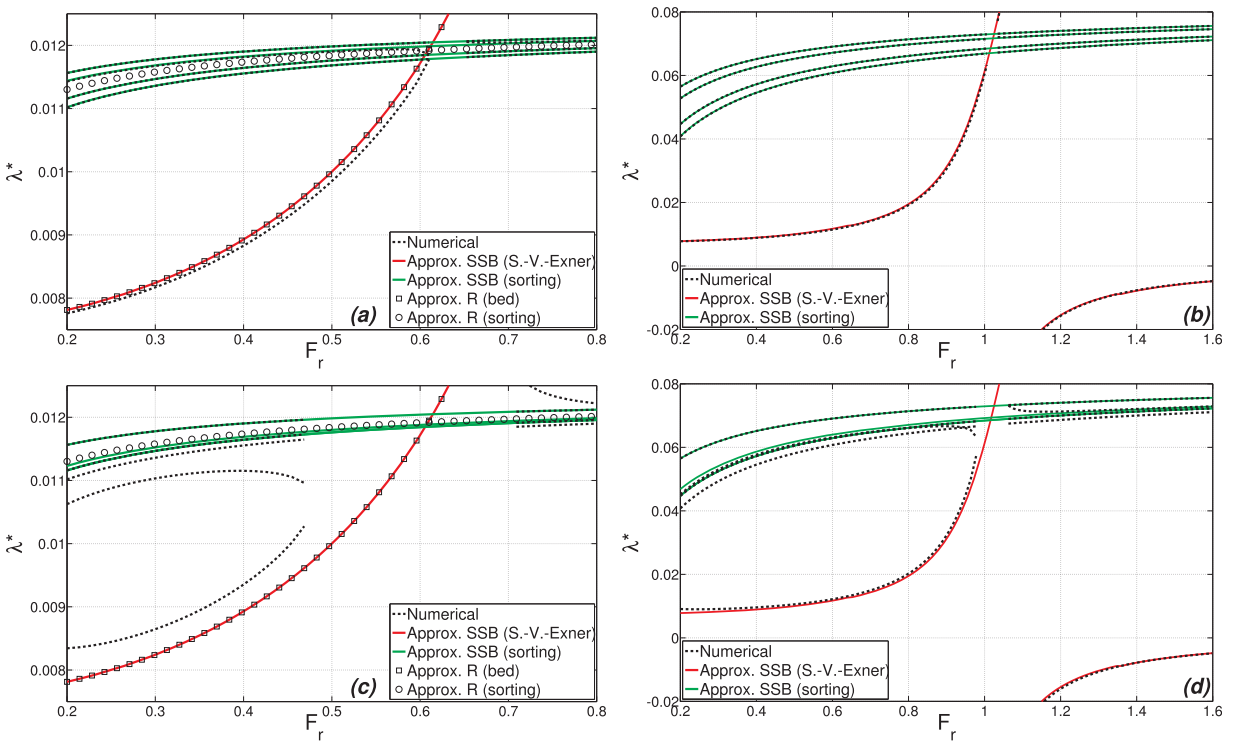

Figure 4. Plot of the system eigenvalues in degradational conditions as function of the Froude parameter, with finer substrate under high-transport conditions. Our estimates and those due to *Ribberink* [1987] are denoted with SSB and R, respectively. $N = 5$ fractions and $\psi = 0.075$ are considered. We use a sharp Gaussian distribution of active layer fractions ($F_{a1} = F_{a5} = 0, F_{a2} = F_{a4} = 0.000004, F_{a3} = 0.999992$. (a, c) Bed form-dominated cases ($L_a^* = 0.2, d_{sm}^* = 0.002, \Delta_d^* = 0.002$). (b, d) Plane-bed cases ($L_a^* = 0.03, d_{sm}^* = 0.01, \Delta_d^* = 0.01$). Figures 4a and 4b: slightly finer sharp distribution of substrate layer fractions ($f_{s1} = f_{s5} = 0, f_{s2} = 0.010986943, f_{s3} = 0.989013056, f_{s4} = 0.000000001$). Figures 4c and 4d: moderately finer sharp distribution of substrate layer fractions ($f_{s1} = f_{s4} = f_{s5} = 0, f_{s2} = f_{s3} = 0.5$).

this case, in the ellipticity range, the reference eigenvalues are not plotted. Our solution, (32), (33), and (36), is not able to automatically detect the ellipticity range and mistakenly provides real eigenvalues even in an elliptic domain. Results are shown in Figure 4. Here bed form-dominated cases are presented in Figures 4a and 4c and plane-bed cases in Figures 4b and 4d, obtained with the same parameter setup as for Figures 3e and 3f, respectively.

Let us focus on Figures 4a and 4b. Under the imposed degradational conditions, the grainsize distribution at the interface between the active and substrate layer f_k^l is equal to that in the substrate (11), which is imposed assuming a sharp Gaussian distribution with mean diameter slightly finer than that in the active layer. In detail, such mean diameter is just 8% finer than that in the active layer, giving rise to the discrete fraction distribution $f_{s1} = f_{s5} = 0, f_{s2} = 0.010986943, f_{s3} = 0.989013056$, and $f_{s4} = 0.000000001$.

In Figure 4a (bed form-dominated conditions), a small region of ellipticity appears around $F_r = 0.63$, where the second-largest Saint-Venant-Exner eigenvalue (red line), here representing the "bed" celerity of *De Vries* [1965], has similar magnitude as the "sorting" wave speeds (green lines). This confirms our findings in section 3.3, by which unconditionally elliptic behavior is found in degradational conditions if the "sorting" eigenvalue has the same magnitude as the second-largest eigenvalue of the Saint-Venant-Exner model and gives a visual explanation of the term "crossing of eigenvalues" adopted by *Sieben* [1997] for this case. Outside the ellipticity region in Figure 4a, our eigenvalue approximation is still accurate. The same behavior is found in the plane-bed case in Figure 4(b), which is characterized by a small ellipticity region around $F_r = 1$.

In Figures 4c and 4d, we use a much finer substrate, having mean diameter 12.5% smaller than that in the active layer, namely $f_{s1} = f_{s4} = f_{s5} = 0$, and $f_{s2} = f_{s3} = 0.5$. In both figures, the ellipticity range is wider compared to that in Figures 4a and 4b and still embraces the region around the intersection of the second Saint-Venant-Exner eigenvalue with the "sorting" eigenvalue. In Figure 4c, the presence of an ellipticity range is seen to alter the reference solution throughout the hyperbolicity range, with respect to the solutions shown

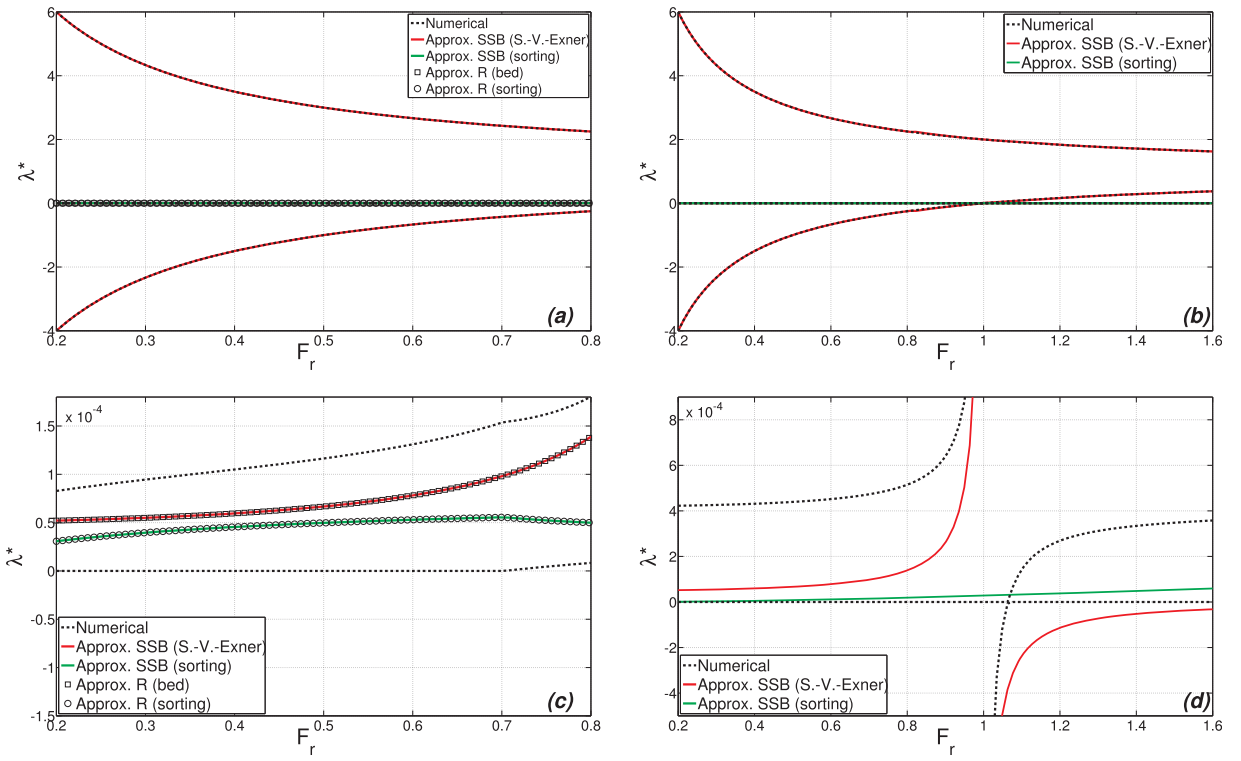

Figure 5. Plot of the system eigenvalues in aggradational conditions as a function of the Froude parameter, under low and partial transport conditions. Our estimates and those due to *Ribberink* [1987] are denoted with SSB and R, respectively. Parameters are $\psi = 0.00005$, $N = 2$, and $F_{a1} = F_{a2} = 0.5$. (a, c) Bed form-dominated cases ($L_a^* = 0.2$, $d_{sm}^* = 0.002$, $\Delta_d^* = 0.002$). (b, d) Plane-bed cases ($L_a^* = 0.03$, $d_{sm}^* = 0.01$, $\Delta_d^* = 0.01$). Figures 5a and 5b: full plot. Figures 5c and 5d: zoom in correspondence of the slowest waves of the set.

in Figure 4a. Both in Figures 4c and 4d, our "sorting" wave estimates turn out to be rather inaccurate even in the hyperbolicity range, since the underlying hypotheses (see the supporting information) are not met.

3.6. System Eigenvalues Under Partial Transport

Under partial transport conditions, i.e., if the flow is not able to transport the coarsest fractions, the overall picture drawn in the previous sections considerably changes. We consider a sediment mixture where only the first P sediment fractions are mobile, with $P < N$, while $N - P$ sediment fractions are immobile. In this case, $N - P$ waves in the system are readily found to have zero speed, i.e., they are steady waves, which retain the associated signal locally, without advecting it through the domain. This happens since $N - P$ null eigenvalues are found in the reduced system matrix (23). These eigenvalues arise from the last $N - P$ lines in the matrix (23), corresponding to the active layer conservation equations for the immobile fractions, which, under the considered partial transport conditions, are linearly dependent on the third line (arising from the Exner equation) and on the lines related to the other $P - 1$ active layer equations.

The wave speed approximations (32), (33), and (36) developed under the hypothesis that all the fractions are mobile, with transport capacities having the same order of magnitude, are now invalid. Therefore, it is no longer possible to split the set of characteristic celerities into the three celerities of the Saint-Venant-Exner model (32) and (33), and additional "sorting" celerities (36).

Since the analysis of the system eigenstructure under partial transport conditions is not easily amenable to analytical treatment, we proceed by numerical computation of the eigenvalues. For simplicity, we restrict our attention to the two-fraction model. Our setup is identical to that used for Figure 2, except for $\psi = 0.00005$, which sets low and partial transport conditions. Results are presented in Figure 5. We consider a bed form-dominated case in Figures 5a and 5c and a plane-bed case in Figures 5b and 5d. Top figures present a full view, while bottom figures provide a zoom to the smallest wave speeds.

Let us initially focus on the bed form-dominated case on the left side of Figure 5. Figure 5a shows that the speeds of the fastest waves in the Saint-Venant-Exner model are not appreciably altered under the assumed

transport conditions, hence the approximations $\lambda^*_{1,2}=1\pm1/F_r$ is still valid. Their physical interpretation is analogous to the high-transport cases: these waves mainly carry changes in the hydrodynamic variables. Focusing on the slowest waves in Figure 5c, we observe that the reference numerical solution (black dashed lines) markedly differs from that reported in Figure 2c for the corresponding high-transport case. Here for Froude numbers smaller than about 0.7, one wave is steady (null celerity) since in that Froude region the coarse fraction is immobile. Conversely, for higher Froude numbers, the coarse fraction is transported and that wave assumes a positive, albeit very small, celerity. Throughout the considered Froude regime, another wave having positive speed is found in the numerical solution. Approximate solutions developed for high-transport conditions, i.e., our solution (32)–(36) and that due to *Ribberink* [1987] are unable to capture the steady wave behavior for $F_r < 0.7$ and underpredict the speed of the fastest of the two waves.

Let us move to the plane-bed case on the right side of Figure 5. Here in the full view of Figure 5b, two celerities in the reference solution closely match the celerities $\lambda^*_{1,2}=1\pm1/F_r$ (32), depicted by red lines, under well-developed sub or supercritical conditions. Switching to Figure 5d, we observe that one wave in the numerical solution (black, dashed line) has null celerity throughout the Froude domain, since, with the adopted setup of sediment diameters and ψ value, the coarsest fraction is always immobile. Under subcritical Froude, the numerical solution yields another wave having positive celerity, as in Figure 5c. Focusing on the supercritical range, a peculiar behavior can be observed. Here approximately for $F_r > 1.07$, no wave having negative celerity is found, which implies that the system does not propagate information in the upstream direction, under the assumed partial transport conditions. This represents a marked difference with the high-transport case studied in the previous sections, where a wave with negative celerity was always found throughout the Froude domain, as can be seen from the eigenvalue pattern in Figure 2d, and with the unisize-sediment case analyzed by *Lyn and Altinakar* [2002]. Such behavior is indeed closer to that of the fixed-bed Saint Venant model, for which information is not conveyed in the upstream direction for $F_r > 1$. Only in the small transcritical region around $F_r = 1$, the celerities $\lambda_{1,2}$ (33) of the Saint-Venant-Exner model better approximate the numerical solution when their absolute magnitude diverges from that of the steady wave.

In the present case of low and partial transport, we cannot link the celerities given by the numerical solution in Figures 5c and 5d to a physical process (i.e., "bed" and "sorting" wave) by simply matching their celerity to that given by our approximate solution. Therefore, the interpretation of the physical role of these waves is not straightforward. Our results show that the fastest between these two waves carries most of sorting effects in the downstream direction (i.e., "sorting" wave behavior), under both well-developed sub and subcritical Froude conditions. The slowest (or steady) wave mainly carries (or locally retains) bed elevation changes ("bed" wave behavior) with negligible to moderate associated sorting.

4. Linearized Problem: Dynamics of Small-Amplitude Waves

In this section, we aim at determining how the dynamics of waves of small amplitude is modified in the mixed-sediment case with respect to the unisize case studied by *Lyn and Altinakar* [2002], with particular reference to the waves affecting the bed elevation profile. In detail, we will highlight the role of the newly introduced "sorting" waves in advecting morphodynamic changes through the domain and we will show that initial localized perturbations in the grainsize distribution of the active layer carried by these waves are able to determine significant bed aggradation or degradation due to the associated bed load gradients.

The study is carried out by application of a linearized analytical solver, which is suitable for studying the propagation of small-amplitude waves. We consider a reference state of variables $\mathbf{Q}_R$, which represents the base flow and transport conditions, and a perturbation of that reference state having infinitesimal amplitude. A linearized problem, having the form

$$\frac{\partial \mathbf{Q}}{\partial t}+\mathbf{A}_R\frac{\partial \mathbf{Q}}{\partial x}=\mathbf{0}\,, \tag{43}$$

is obtained from the nonlinear system (20) by freezing the system matrix around the values of variables given by the reference state, i.e., $\mathbf{A}_R=\mathbf{A}(\mathbf{Q}_R)$. In the following, the reference values will be indicated with subscript R. The analytical solution to the linearized problem governed by (43) can be computed from the eigenstructure of the matrix $\mathbf{A}_R$, which is uniquely determined once the dimensionless parameters on the right-hand side of (37) are specified for the reference state. Details on the solution algorithm are given in the supporting information.

4.1. Simulation Setup

We assume as initial condition the reference state throughout the domain, except for a localized smooth perturbation of the grainsize distribution of the active layer in the proximity of $x = 0$. In detail, the reference grainsize distribution is equal for all fractions, i.e., $F_{akR} = 1/N$. For one of the fractions in the mixture, the Kth fraction, we prescribe a Gaussian longitudinal perturbation of equal distribution

$$F_{aK}(x,0) = \frac{1}{N} + A_F \exp\left(-\left(\frac{x}{\sqrt{2}\sigma}\right)^2\right), \tag{44}$$

where $-1/N < A_F < 1-1/N$ is the amplitude of the perturbation. Such amplitude is assumed to be small to comply with the hypothesis of linearity. Positive (negative) values of A_F denote a higher (smaller) content of the Kth fraction around $x = 0$. The content of the other fractions is given by

$$F_{ak}(x,0) = \frac{1-F_{aK}(x,0)}{N} \quad \text{for } k \neq K. \tag{45}$$

The initial grainsize distribution in the substrate is equal to that in the active layer, i.e., $f_{sk}(x,z,0) = F_{ak}(x,0)$. Therefore, no elliptic behavior is expected to occur in computations. The initial bed profile is flat throughout the domain, except for a localized perturbation around $x = 0$ given by a Gaussian hump, having infinitesimal amplitude A_η and standard deviation σ:

$$\eta(x,0) = A_\eta \exp\left(-\left(\frac{x}{\sqrt{2}\sigma}\right)^2\right). \tag{46}$$

Since the Gaussian function fastly decreases and vanishes for $|x| > 3\sigma$, the bed and active layer setup smoothly connect with the reference state. Flow is from negative to positive x. The initial condition for flow depth is prescribed assuming constant specific discharge q, by analytically integrating the inviscid backwater profile

$$\frac{\partial h}{\partial x} = \frac{1}{1-F_r^2}\left(-\frac{\partial \eta}{\partial x}\right), \tag{47}$$

with boundary condition $h(L/2,0) = h_R$ or $h(-L/2,0) = h_R$ under sub or supercritical conditions, respectively.

4.2. Results

Here we apply our linearized solver to three test cases, under high-transport conditions. In Tests 1 and 2, we will consider a two-fraction setup (one active layer equation) under sub and supercritical flow conditions (section 4.2.1) using various kinds of initial perturbation under high-transport conditions (low grainsize selectivity). Finally, in Test 3 (section 4.2.3), we will analyze the wave dynamics for a five-fraction mixture.

The initial bed profile is prescribed by (46) using the dimensionless quantities

$$A_\eta^* = \frac{A_\eta}{h_R}, \quad \sigma^* = \frac{\sigma}{u_R t^{out}}, \tag{48}$$

in which $u_R = q_R/h_R$ is the reference flow velocity. The initial active layer grainsize distribution is set using (44) and (45) after choosing A_F and selecting the Kth fraction in (44). The substrate is assumed to have the same initial grainsize distribution as the active layer. The solution profiles will be presented using the dimensionless variables

$$h^* = \frac{h-h_R}{a_\eta}, \qquad \eta^* = \frac{\eta}{a_\eta}, \qquad F_{ak}^* = \frac{F_{ak}-1/N}{a_F}, \tag{49}$$

where $a_\eta = \max\left(A_\eta, 10^{-5}h_R\right)$ and $a_F = \max\left(|A_F|, 10^{-3}\right)$ are identical to the perturbation amplitude except for a correction in case of vanishing imposed perturbation. We will use the dimensionless abscissa

$$x^* = \frac{x}{u_R t^{out}}. \tag{50}$$

The proposed dimensionless solution is independent from t^{out} and u_R.

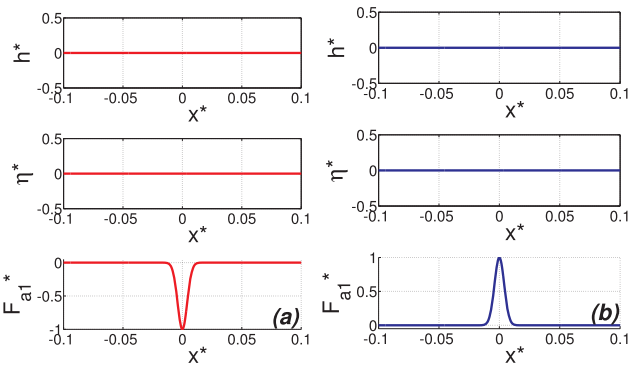

Figure 6. (a) Test 1.1 and (b) Test 1.2: initial condition.

4.2.1. Test 1: Influence of Sorting on the Bed Profile

In this test, we initially set a flat bed, i.e., $A_\eta = 0$ in (46), and the resulting backwater profile (47) is flat as well, i.e., equal to the reference depth h_R throughout the domain. Concerning the grainsize distribution in the active layer, we consider two setups. In Test 1.1, we impose a coarser perturbed active layer setup than the surrounding bed, while in Test 1.2 a finer one. This is set using the value $A_F = -10^{-3}$ in Test 1.1 and $A_F = 10^{-3}$ in Test 1.2 with respect to the first fraction ($K = 1$), with $\sigma^* = 0.004$. The initial condition for scaled depth h^*, bed elevation η^*, and active layer content of the first fraction F^*_{a1} (49) is graphically represented in Figure 6. Here Figure 6a refers to Test 1.1 and Figure 6b to Test 1.2. In both figures, the reference value $F^*_{a1} = 0$ corresponds to equal fraction content in the reference state $F^*_{a1} = 0.5$, while the Gaussian peak value $F^*_{a1} = \mp 1$ denotes the perturbed value $F_{a1} = 0.5 \mp 10^{-3}$.

The initial grainsize distribution in the active layer is characterized by an initial localized perturbation around $x^* = 0$. Therefore, although the initial condition represents an equilibrium state for the hydrodynamic variables (i.e., constant discharge and depth throughout the domain), it is associated with an imbalanced setup of total bed load around $x^* = 0$, due to the local perturbation in the grainsize distribution of the active layer. At $t = 0$, a movable-bed computation starts and such imbalance triggers four waves, which eventually travel through the domain at the speed and in the direction given by (32) and (36). See also Figure 2 for a graphical representation of the wave speeds of the two-fraction model.

We use (42) to set the reference dimensionless sediment diameters, with $d^*_{smR} = 0.01$ and $\Delta^*_{dR} = 0.015$, giving $d^*_{s1R} = 0.0025$ and $d^*_{s2R} = 0.0175$. The active layer setup refers to a plane-bed case with $L^*_{aR} = 4d^*_{smR} = 0.04$. We set $\psi_R = 0.0075$, corresponding to relatively high sediment transport conditions. Concerning the Froude regime, we consider a subcritical case with $F_{rR} = 0.65$ and a supercritical case with $F_{rR} = 1.35$, for both Tests 1.1 and 1.2.

Results are presented in Figure 7. Figures 7a and 7b refer to Test 1.1, while Figures 7c and 7d to Test 1.2. Subcritical cases are presented on the left side (a) and (c), supercritical cases on the right side (b) and (d). Let us initially focus on the solution profiles to Test 1.1 in Figures 7a and 7b. Under both sub and supercritical flow conditions, four traveling perturbations, corresponding to the four waves, are produced.

Three of these waves travel at similar speed as those of the Saint-Venant-Exner model in the respective Froude regime (32). Among them, the fastest, downstream-traveling wave which propagates at speed $\lambda^* = 1 + 1/F_r$ is located at $x^* \simeq 2.54$ and $x^* \simeq 1.74$ in the sub and supercritical case, respectively. However, the associated perturbations in h^* and η^* are in practice not noticeable in a full view due to insufficient amplitude. Hence, the corresponding region is left out of the plot. The second-fastest wave in absolute value, traveling at speed $\lambda^* = 1 - 1/F_{rR}$ in the upstream direction ($x^* \simeq -0.55$) under subcritical conditions and in the downstream direction ($x^* \simeq 0.26$) under supercritical conditions, carries a modest perturbation in depth and a negligible bed change. The slowest among these waves travels in the downstream direction ($x^* \simeq 0.01$) in the subcritical case (Figure 7a) and in the upstream direction ($x^* \simeq -0.01$) in the supercritical case (Figure 7b) and carries a major bed elevation change and associated flow depth change. Thus, the role of these three waves in advecting bed and free-surface changes is entirely analogous to that found for the unisize-sediment case by *Lyn and Altinakar* [2002]. In Figure 7, none among these three Saint-Venant-Exner waves carries any significant perturbation in the volume fraction content of the active layer F_{a1}.

The remaining, downstream-traveling wave, located at $x^* \simeq 0.055$ in Figures 7a and 7b, is the only wave associated with the advection of significant changes in the grainsize distribution of the active layer, which justifies the adoption of the name of "sorting" wave. The displacement of this wave is thus clearly indicated by a perturbation of the active layer volume fractions at $x^* \simeq 0.055$, almost retaining the initial amplitude $F^*_{a1} = -1$. Together with perturbations in the grainsize distribution, the "sorting" wave carries nonnegligible bed elevation changes, which are caused by bed load gradients associated with spatial variations in the volume fraction content in the active layer, and the resulting major perturbations in water depth.

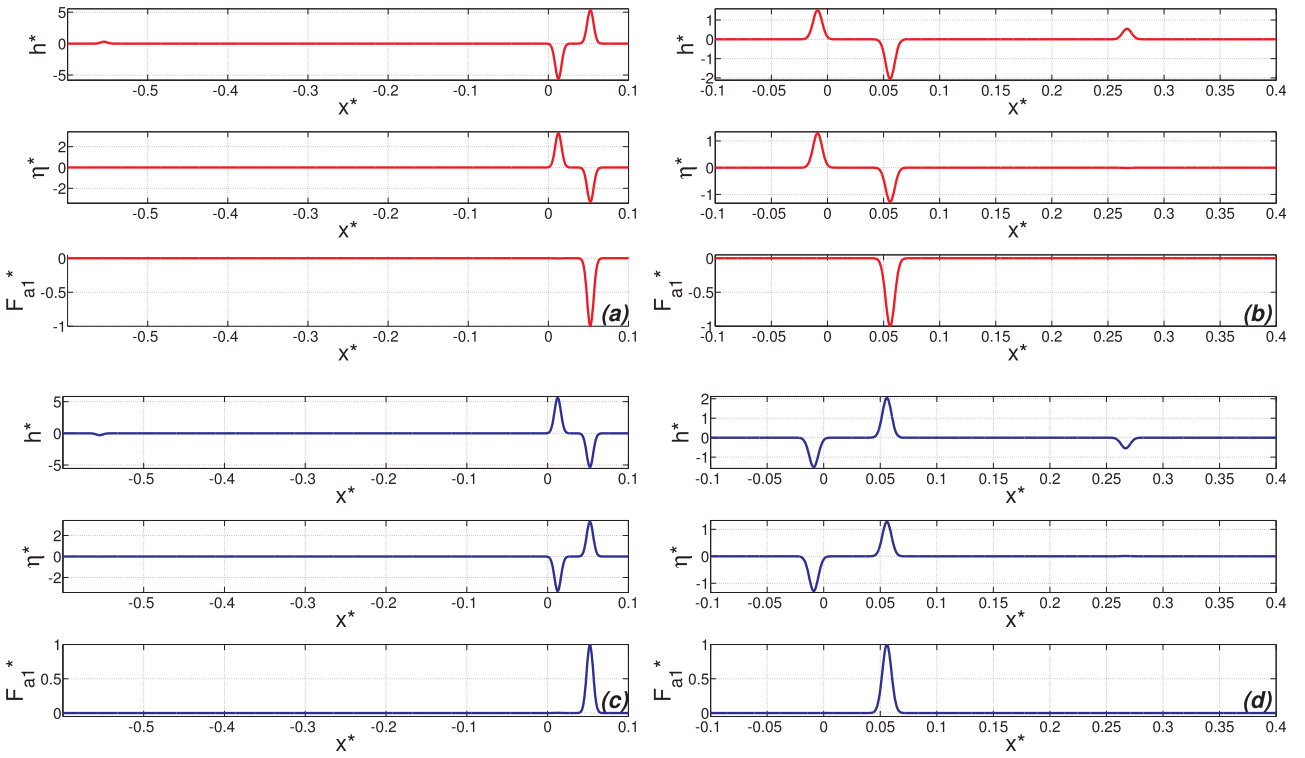

Figure 7. Test 1.1 and 1.2: wave propagation governed by the Saint-Venant-Hirano model for two fractions, induced by perturbation of the grainsize distribution in the active layer. $\psi_R = 0.0075$, $N = 2$, $d^*_{s1R} = 0.0025$, $d^*_{s2R} = 0.0175$, and $L^*_{aR} = 0.04$. (a, b) Test 1.1, perturbation amplitude of the first fraction content $A_F = -10^{-3}$ (localized initial coarsening); (c, d) Test 1.2, perturbation amplitude of the first fraction content $A_F = 10^{-3}$ (localized initial fining). Figures 7a and 7c: subcritical regime ($F_{rR} = 0.65$); Figures 7b and 7d: supercritical regime ($F_{rR} = 1.35$). Perturbation: $A^*_\eta = 0$, $\sigma^* = 0.004$. The flow depth and bed elevation profile are nondimensionalized with $a_\eta = 10^{-5} h_R$.

Immediate consequence of the introduction of a two-fraction mixture with respect to the unisize-sediment case is thus, under subcritical conditions, that bed elevation changes are advected not only along the "bed" wave λ^*_3 (32) but also along the faster "sorting" characteristic direction (36). Under supercritical conditions, the "sorting" wave introduces a novel downstream-propagating effect on bed elevation, in addition to the upstream-propagating "bed" wave of the unisize-sediment model.

We now focus on the amplitude of the perturbations in η^* associated with the "bed" and "sorting" waves and analyze why they are negative (degradation) or positive (aggradation). This can be explained considering the initial perturbation of the grainsize distribution in the active layer. In the present test, the initial imbalance causing wave propagation is given by reduced bed load transport around $x^* = 0$ associated with local coarsening. A negative (positive) bed load gradient is produced upstream (downstream) of the initial perturbation and is associated by the Exner equation (3) to temporal increase (decrease) in bed elevation. This perturbation in bed load is then advected along the "sorting" wave ($x^* \simeq 0.055$), thus determining an associated downstream-traveling scour in the bed profile. To retain the sediment mass balance, the scour is compensated by the formation of a sediment hump, which is advected along the "bed" wave. Sorting is thus shown here to be very effective in triggering perturbations of bed elevation, starting from a minimal initial perturbation in the grainsize distribution of the active layer ($A_F = -10^{-3}$).

A different behavior can be obtained with a different initial perturbation. In Test 1.2, the initial bed shows local initial fining ($A_F = 10^{-3}$), giving an opposite perturbation of total bed load with respect to that in Test 1.1. Since the two tests have identical reference state $\mathbf{Q}_R$ and matrix $\mathbf{A}_R$, they are characterized by identical wave speeds under the assumption of linearity.

Results for Test 1.2 are shown in Figures 7c and 7d. In the bed profile, degradation (aggradation) in Test 1.2 corresponds to aggradation (degradation) in Test 1.1. This behavior can be explained by analogous arguments as those used for Test 1.1 and highlights the influence of the initial perturbation on the final profiles.

Finally, we have performed an additional test analogous to Test 1.2, but with increased grainsize selectivity, which was obtained by reducing the ψ value, i.e., the total bed load transport. Our results, not graphically presented here, demonstrate that, under subcritical flow, the amplitude of the perturbation in the grainsize distribution of the active layer F_{a1} carried by the downstream-traveling "bed" wave increases with increasing size selectivity, although the faster "sorting" wave always carries the great majority of the initial imposed perturbation in F_{a1}. Under supercritical flow instead, even with increased grainsize selectivity, the amplitude of the perturbation in the grainsize distribution of the active layer carried by the "bed" wave in the upstream direction always remains infinitesimal, and a perturbation in F_{a1} which almost retains the initially imposed unit amplitude is seen to travel along the "sorting" eigenvalue in the downstream direction. This confirms the conclusion that most of sorting effects are always conveyed in the downstream direction, regardless of the Froude and sediment transport regime.

4.2.2. Test 2: Influence of Bed Perturbations on Sorting

Having shown that sorting has a considerable feedback on bed elevation changes, we aim here at showing that the opposite feedback is much less pronounced and hardly noticeable. We solve an identical problem as in Tests 1.1 and 1.2 in the previous section, but with a different initial condition. We consider an infinitesimal bed hump having amplitude $A_\eta = 10^{-5} h_R$ (46) without any active layer perturbation, i.e., $A_F = 0$ in (44). Thus, in this case, the bed load imbalance triggering wave propagation is caused by flow acceleration (deceleration) in the initial backwater profile (47) under subcritical (supercritical) conditions. For further clarification, we refer the reader to *Lyn and Altinakar* [2002], who have analyzed the wave pattern arising from this initial setup in the unisize-sediment case.

Results are displayed in Figures 8a (subcritical case) and 8b (supercritical case), where the region occupied by the fastest wave, showing minimal perturbations in variables, has been left out of the plot. Since the reference matrix $\mathbf{A}_R$ and its eigenstructure are identical to those in Tests 1.1 and 1.2, the wave celerities do not change. However, the present wave pattern significantly differs from that given in Figure 7. Under both sub and supercritical conditions (see Figure 8), the only wave having any impact on bed elevation is the bed wave λ_3^* (32), which carries the initial bed perturbation without noticeable amplification or damping with respect to the initial condition.

The "sorting" wave at $x^* \simeq 0.055$ now carries a very small perturbation in the grainsize distribution of the active layer (not visually noticeable in Figure 8) and thus is not able to trigger any significant river bed change. Other computations (figures not reported here) show that such feedback remains relatively small and hardly noticeable even by adopting a setup characterized by higher grainsize selectivity.

The dynamics of waves having an impact on the bed profile with this initial condition very closely resembles that predicted by the Saint-Venant-Exner model for unisize sediment [*Lyn and Altinakar*, 2002]. Thus, a very small feedback effect due to gradients in bed elevation and hydrodynamic variables shall be expected on sorting processes, at least for the smooth problem described here.

4.2.3. Test 3: Multiple-Fraction Mixtures and Sorting Wave Separation

In this test, we analyze the bed profiles obtained using a multiple-fraction mixture ($N = 5$ fractions). Fraction diameters are assigned using (42) with $d^*_{smR} = 0.02$ and $\Delta^*_{dR} = 0.025$. We consider a subcritical test case with $F_{rR} = 0.65$, in which all waves are expected to travel at distinct pace as shown in section 4.2.1. We set $\psi_R = 0.01$ and consider a plane-bed case with $L^*_{aR} = 3d^*_{smR} = 0.06$. The bed and flow depth profile are initially flat ($A^*_\eta = 0$). Concerning the initial perturbation of the grainsize distribution in the active layer (44), we set amplitude $A_F = 10^{-3}$ and longitudinal extent $\sigma^* = 0.00035$. We consider two different setups: in Test 3.1, we apply the perturbation to the second fraction, which results in a localized initial increase in total bed load, and in Test 3.2 to the third fraction, which results in an initial decrease in total bed load.

Results are displayed in Figure 9a for Test 3.1 and in Figure 9b for Test 3.2 in terms of profiles for the variables h^*, η^*, and F^*_{ak} (49), including the profiles of fractions from 1 to 4. For clarity, only the region corresponding to the waves having significant impact on bed elevation, namely the "bed" wave and the four "sorting" waves, is shown. We have verified that the fastest and slowest wave, not shown in the figure, carry negligible bed changes, as in the two-fraction case of Test 1.

In both sides in Figure 9, the "bed" wave is revealed by degradation of the bed profile at $x^* \simeq 0.016$, while the four faster "sorting" waves are indicated by positive and negative peaks of the volume fraction content in the active layer. These waves, traveling in the downstream direction at the speed given by the distinct

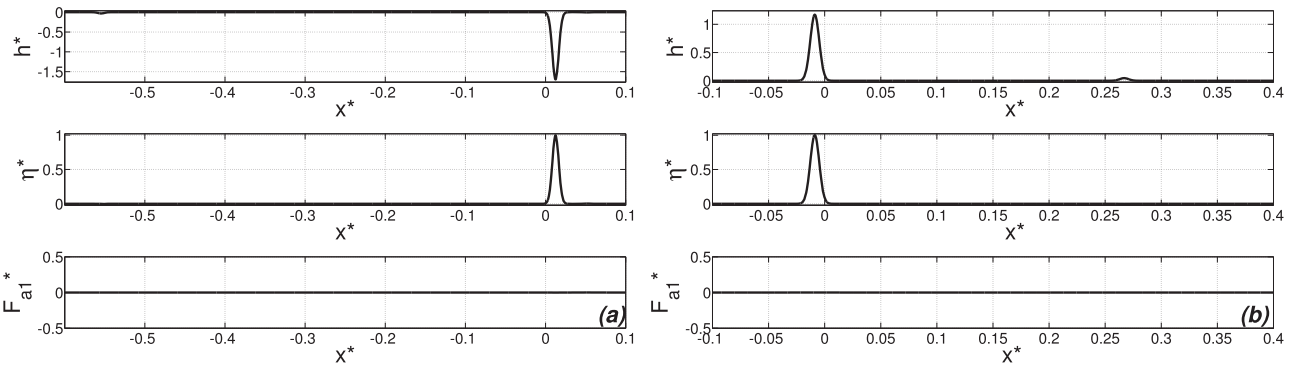

Figure 8. Test 2: wave propagation governed by the Saint-Venant-Hirano model for two fractions, induced by an initial bed hump. $\psi_R = 0.0075$, $N = 2$, $d^*_{s1R} = 0.0025$, $d^*_{s2R} = 0.0175$, and $L^*_{aR} = 0.04$. (a) Subcritical regime ($F_{rR} = 0.65$) and (b) supercritical regime ($F_{rR} = 1.35$). Perturbation: $A^*_\eta = 10^{-5}$ and $\sigma^* = 0.004$. The active layer fraction profile is scaled with $a_F = 10^{-3}$.

"sorting" eigenvalues (36), have separated. As for the two-fraction case, each of these waves is associated with local perturbation of the bed elevation profile due to the total bed load gradients associated with perturbations in the volumetric fraction content in the active layer. The resulting, downstream-traveling perturbations of bed elevation also generate perturbations of the flow depth profile at $x^* \simeq 0.016$. Thus, by including multiple fractions in the model, the hydromorphodynamic profiles become significantly more complex than those for two fractions, even adopting the present linearized solution approach. It is also seen that all the "sorting" waves carry perturbations of the volume fraction content in all fractions. Comparing the two sides in Figure 9, the solution profiles in all variables are seen to significantly depend on the initial condition.

This test shows that in the case of multiple "sorting" waves, which arise due to multiple active layer equations in case the number of size fractions exceeds 2, each "sorting" wave induces a distinct perturbation of the bed profile. With respect to the previously considered two-fraction case, here multiple "sorting" waves are seen to separate while traveling downstream at distinct pace, and to create multiple degradational and aggradational patterns having significant amplitude. In practical cases, the number of fractions employed in the discretization of a granulometric curve is thus expected to significantly affect the propagation speed of disturbances and the final river bed configuration.

5. Discussion

For the purpose of analysis, the model has been made inviscid by neglecting the frictional source terms in the momentum equation. This is a reasonable assumption when focusing on the small-amplitude waves that develop and propagate over short time and length scales (a few seconds and meters in real streams),

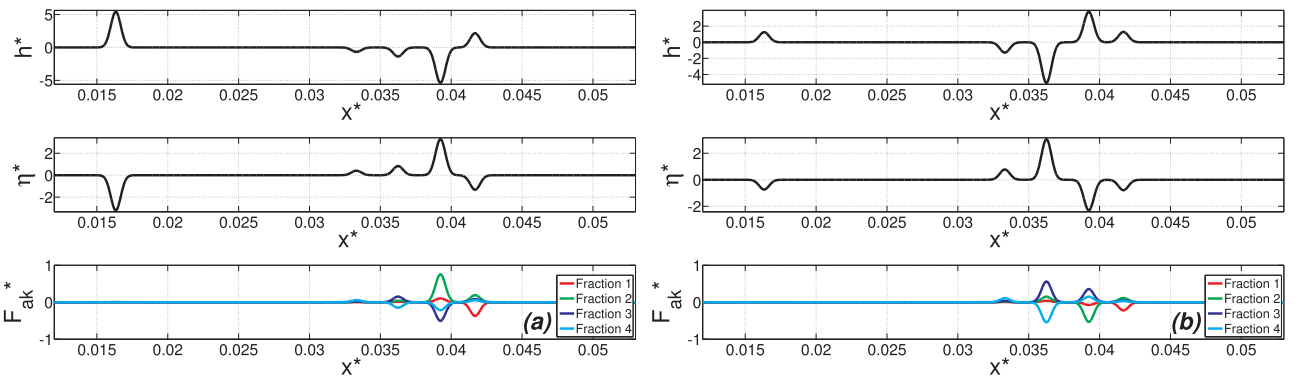

Figure 9. Test 3: wave propagation governed by the Saint-Venant-Hirano model for multiple fractions, under subcritical flow conditions. $\psi_R = 0.01$, $N = 5$, $d^*_{smR} = 0.02$, $\Delta^*_{dR} = 0.025$, and $L^*_{aR} = 0.06$. Perturbation $A^*_\eta = 0$, $A_F = 10^{-3}$, and $\sigma^* = 0.00035$. (a) Test 3.1, perturbation applied to the second fraction and (b) Test 3.2, perturbation applied to the third fraction. The water depth and bed elevation profile are nondimensionalized with $a_\eta = 10^{-5} h_R$.

as was done by, e.g., *Lyn* [1987], *Lyn and Altinakar* [2002], and *Ribberink* [1987]. In the unisize-sediment case, *Lyn and Altinakar* [2002] have analyzed the impact of this assumption by performing numerical computation on the propagation of small-amplitude wave issuing by a bed hump, with and without accounting for friction. They have found that, in the solution including friction, the basic features of the linear problem can still be discerned in spite of some marked distortions in the bed profile. In detail, for short times, the "bed" wave assumes an amplitude quite close to that predicted by the inviscid linear solution and the wave celerities are not significantly altered. Based on this, we consider the linearized inviscid solutions of this paper reliable provided the restrictions with respect to short time and spatial scales and small amplitude of perturbations are met.

It is worth noticing that several attempts to extend the validity of linear inviscid solutions beyond the limit of these hypotheses are found in the literature. For instance *Mosselman et al*. [2008] and *Sloff and Mosselman* [2012] have used an approximation to the "bed" and "sorting" celerities of the inviscid model to study the propagation of morphodynamic changes at the reach scale. This approach is useful for simple conceptual interpretation but can only provide rough estimates in a quantitative sense. In fact, frictional source terms should be introduced while considering hydromorphodynamic changes affecting the river long profile. These "long waves" could be studied using a perturbation approach, in a similar manner as was done by *Lanzoni et al*. [2006] and *Fasolato et al*. [2009] for unisize sediment. Further work on this point is needed.

Iseya and Ikeda [1987], *Kuhnle and Southard* [1988], and *Recking et al*. [2009] have shown that bed load transport, measured at the downstream end of a flume with constant hydraulic conditions and constant sediment feed composed of mixed sediment, presents an inherent fluctuating behavior, which, according to *Recking et al*. [2009], is correlated with fluctuations of the bed slope. This may suggest legacies with our analytical solution of the Saint-Venant-Hirano model in the multiple-fraction case in Figure 9, where pulsations in total bed load are associated with the traveling perturbations in the grainsize distribution of the active layer and in the bed profile. However, in spite of these analogies, some behavioral differences between the outcomes of laboratory experiments and of our analysis must be remarked. The periodicity reported by *Recking et al*. [2009] includes a continuous spectrum of time scales, i.e., from the very low frequencies due to complex long-term surface changes to the intermediate frequencies of bed load sheets, until the high frequency of changes happening within bed load sheets. The one-dimensional Saint-Venant-Hirano model in our analysis is incapable of reproducing the instability mechanisms which are responsible of bed load sheets, for which the more complex, two-dimensional model proposed by *Seminara et al*. [1996] is needed. Thus, the fluctuations carried by the "sorting" waves in our linearized analysis could possibly only be associated with the fastest variations in the study of *Recking et al*. [2009], which however have been filtered out in their analysis. Mismatch is also found in the amplitude of the signal, since the infinitesimal amplitude of perturbations in our linear solution is not compatible with the huge amplitude of bed load fluctuations in the experiments. It is then an open question whether at least the highest frequency perturbations in the experiments could be modeled as the result of some instability mechanism triggered by the small-amplitude fluctuations studied in this paper, thus producing finite-amplitude perturbations having the required frequency. This could be analyzed using a numerical implementation of the present model in a multiple-fraction setup, so as to remove the hypothesis of linearity.

Our analysis, as well as the previous results of *Ribberink* [1987] and *Sieben* [1997], reveals that the model may loose its hyperbolic character under degradational conditions, thus denoting ill-posedness in those cases. This may suggest that the purely advective behavior of the Exner and Hirano equations used in conjunction with usual bed load transport relations is a too crude approximation of the physics. In fact, recent analysis of sediment transport has shown that the bed load flux also includes a diffusive component [*Ancey and Heyman*, 2014; *Furbish et al*., 2012; *Ballio et al*., 2014]. In future work, it might be worth analyzing whether the possibly ill-posed behavior of the Saint-Venant-Hirano model can be cured by introducing these diffusion terms in the definition of bed load discharge, adopting a similar approach to that proposed by *Gray and Ancey* [2011] for another system of PDEs.

In fact, most of the advances presented in this paper, which belong to the improvement of the mathematical understanding of continuity models for mixed sediment, pave the way for improvement in numerical solution techniques and applications. The linearized solutions presented in section 4 can serve as benchmark for assessing the convergence and accuracy of numerical models. Moreover, detailed knowledge of the propagation direction and speed of hydrodynamic and morphodynamic perturbations, as described by

the system of governing equations, can be used to properly impose the boundary conditions. For instance, the fact that, as shown by the linearized solution, perturbations in the grainsize distribution in the active layer mainly travel in the downstream direction, suggests that physically meaningful conditions for these variables shall be imposed at the upstream boundary. Finally, the developed matrix-vector (nonconservative) formulation is suitable for the application of modern path-conservative methods [*Dal Maso et al*., 1995; *Parés*, 2006], for instance those of *Canestrelli et al*. [2009] and *Dumbser and Toro* [2011]. Since our formulation preserves the full unsteadiness of the mathematical problem and all the equations are solved simultaneously, the resulting numerical algorithms will be optimal for handling trans- and supercritical flows, as pointed out by *Sieben* [1997], and the transitions between them.

6. Conclusions

In this paper, we have studied the system of partial differential equations arising from the coupling of the unsteady Saint-Venant model with the Hirano active layer model for mixed-sediment morphodynamics. After rewriting the system of PDEs in matrix-vector form, we have analyzed the system eigenstructure, in order to study the propagation of small-amplitude hydromorphodynamic waves as described by the model.

The two distinctive features of the present analysis are that full unsteadiness of the problem is retained and that multiple size fractions are considered, thus accounting for grainsize selectivity of bed load transport. This allows us to develop approximations to all the characteristic speeds in the model written for an arbitrary number of fractions under any Froude regime. Our analysis focuses on the $N-1$ characteristic directions, which are described by the model set for N fractions, in addition to the three characteristic directions of the unisize-sediment case. Under high sediment transport conditions, i.e., when all the size fractions are transported, we have analytically shown that all the $N-1$ "sorting" celerities are positive, denoting downstream-traveling waves, and that if grainsize selectivity is assumed, these celerities are distinct, denoting waves which travel at different pace. By retaining individual equations for each size fraction in the analysis, we have also been able to analyze the case of partial transport. In this case, we have found a number of steady waves (i.e., having null celerity) equal to the number of immobile fractions.

We have assessed the hyperbolicity of the model analytically in the two-fraction setup, retaining grainsize selectivity. We have proven that the system is strictly hyperbolic in aggradational conditions and when the active layer degrades into a coarser substrate, whereas it may be elliptic if degradation takes place into a finer substrate. In the latter case, the model is unsuitable for morphodynamic predictions, because an elliptic problem would also require a boundary condition in time from future to past, which is physically meaningless.

By means of linearized solutions, we have studied the impact of the "sorting" waves on the propagation of perturbations in bed elevation. We have shown that a localized change in the grainsize distribution of the active layer is mainly advected in the downstream direction along the "sorting" characteristic directions. The resulting imbalances in total bed load trigger downstream-traveling bed perturbations, which are conveyed along the same waves together with the above-mentioned perturbations in the grainsize distribution of the active layer. The overall sediment mass balance is then preserved by the creation of another bed perturbation, which travels at slower pace in the downstream (upstream) direction under subcritical (supercritical) conditions along the bed wave. Since the "sorting" waves are usually faster than the "bed" wave, the mixed-sediment model predicts that perturbations in riverbed elevation propagate at faster pace than in the unisize-sediment case governed by the Saint-Venant-Exner model. Moreover, under supercritical conditions, the "sorting" wave of the mixed-sediment model introduces a novel downstream-propagating effect on bed elevation, in addition to the upstream-propagating "bed" wave of the unisize-sediment model. Conversely, a smooth initial perturbation of bed elevation and hydrodynamic variables does not trigger significant "sorting" effects, and the resulting perturbation in the grainsize distribution of the active layer keeps modest even in case of strong grainsize selectivity.

Finally, in a multiple-fraction case ($N > 2$), the distinct "sorting" waves carry distinct downstream-traveling associated perturbations of the bed elevation. The final pattern of bed perturbations is thus shown to markedly depend on the number of sediment fractions which is employed in the discretization of the granulometric curve. At present, our analysis is not able prescribe the most convenient discretization of a granulometric curve in practical cases, but only to foresee its consequences in terms of wave propagation. In future work, this issue could be thoroughly explored employing a numerical implementation of the model, by comparison with detailed laboratory data.

Appendix A: The System Matrix in Extended Form

We rewrite the system matrix **A** (22) in extended form, i.e., not making use of indices *k* and *l*. We use the block notation

$$\mathbf{A}=\left[\begin{array}{c|c|c} \mathcal{E}1 & \mathcal{E}2 & \mathbf{0}_{3\times(N-1)} \\ \hline \mathcal{A}1 & \mathcal{A}2 & \mathbf{0}_{(N-1)\times(N-1)} \\ \hline \mathcal{S}1 & \mathcal{S}2 & \mathbf{0}_{(N-1)\times(N-1)} \end{array}\right]. \tag{A1}$$

Here **0** are the matrices containing only 0 entries, whose size is indicated by their subscripts, and the other blocks are given by

$$\mathcal{E}1=\begin{bmatrix} 0 & 1 & 0 \\ gh-u^2 & 2u & gh \\ \dfrac{\partial q_b}{\partial h} & \dfrac{\partial q_b}{\partial q} & 0 \end{bmatrix}, \qquad \mathcal{E}2=\begin{bmatrix} 0 & \cdots & 0 \\ 0 & \cdots & 0 \\ \dfrac{\partial q_b}{\partial M_{a1}} & \cdots & \dfrac{\partial q_b}{\partial M_{aN-1}} \end{bmatrix}, \tag{A2}$$

$$\mathcal{A}1=\begin{bmatrix} \dfrac{\partial q_{b1}}{\partial h}-f_1^l\dfrac{\partial q_b}{\partial h} & \dfrac{\partial q_{b1}}{\partial q}-f_1^l\dfrac{\partial q_b}{\partial q} & 0 \\ \cdots & \cdots & \cdots \\ \dfrac{\partial q_{bN-1}}{\partial h}-f_{N-1}^l\dfrac{\partial q_b}{\partial h} & \dfrac{\partial q_{bN-1}}{\partial q}-f_{N-1}^l\dfrac{\partial q_b}{\partial q} & 0 \end{bmatrix}, \tag{A3}$$

$$\mathcal{A}2=\begin{bmatrix} \dfrac{\partial q_{b1}}{\partial M_{a1}}-f_1^l\dfrac{\partial q_b}{\partial M_{a1}} & \cdots & \dfrac{\partial q_{b1}}{\partial M_{aN-1}}-f_1^l\dfrac{\partial q_b}{\partial M_{aN-1}} \\ \cdots & \cdots & \cdots \\ \dfrac{\partial q_{bN-1}}{\partial M_{a1}}-f_{N-1}^l\dfrac{\partial q_b}{\partial M_{a1}} & \cdots & \dfrac{\partial q_{bN-1}}{\partial M_{aN-1}}-f_{N-1}^l\dfrac{\partial q_b}{\partial M_{aN-1}} \end{bmatrix}, \tag{A4}$$

$$\mathcal{S}1=\begin{bmatrix} f_1^l\dfrac{\partial q_b}{\partial h} & f_1^l\dfrac{\partial q_b}{\partial q} & 0 \\ \cdots & \cdots & \cdots \\ f_{N-1}^l\dfrac{\partial q_b}{\partial h} & f_{N-1}^l\dfrac{\partial q_b}{\partial q} & 0 \end{bmatrix}, \quad \mathcal{S}2=\begin{bmatrix} f_1^l\dfrac{\partial q_b}{\partial M_{a1}} & \cdots & f_1^l\dfrac{\partial q_b}{\partial M_{aN-1}} \\ \cdots & \cdots & \cdots \\ f_{N-1}^l\dfrac{\partial q_b}{\partial M_{a1}} & \cdots & f_{N-1}^l\dfrac{\partial q_b}{\partial M_{aN-1}} \end{bmatrix}. \tag{A5}$$

Acknowledgments
The first author is employed under the Aspasia scholarship 015.007.051 of the Netherlands Organization for Scientific Research (NWO). The authors thank E. Mosselman (Deltares, Delft, Netherlands) for fruitful discussion and the three referees—two anonymous reviewers and J. S. Ribberink (University of Twente, Enschede, Netherlands)—for their constructive comments and remarks, which definitely helped to improve the clarity and the content of this article.

References

Ancey, C., and J. Heyman (2014), A microstructural approach to bed load transport: Mean behaviour and fluctuations of particle transport rates, *J. Fluid Mech.*, *744*, 129–168.

Armanini, A., and G. Di Silvio (1998), A one-dimensional model for the transport of a sediment mixture in non-equilibrium conditions, *J. Hydraul. Res.*, *26*, 275–292.

Ashida, K., and M. Michiue (1971), An investigation of bed degradation downstream of a dam, in *14th Congress IAHR*, pp. 247–255, Int. Assoc. of Hydrol. Sci., Wallingford, U. K.

Ashida, K., and M. Michiue (1972), Study on hydraulic resistance and bedload transport rate in alluvial streams, *Trans. Jpn. Soc. Civ. Eng.*, *206*, 59–69.

Ballio, F., V. Nikora, and S. E. Coleman (2014), On the definition of solid discharge in hydro-environment research and applications, *J. Hydraul. Res.*, *52*(2), 173–184.

Blom, A., and G. Parker (2004), Vertical sorting and the morphodynamics of bedform-dominated rivers: A modeling framework, *J. Geophys. Res.*, *109*, F02007, doi:10.1029/2003JF000069.

Blom, A., J. S. Ribberink, and G. Parker (2008), Vertical sorting and the morphodynamics of bed form-dominated rivers: A sorting evolution model, *J. Geophys. Res.*, *113*, F01019, doi:10.1029/2006JF000618.

Canestrelli, A., A. Siviglia, M. Dumbser, and E. Toro (2009), Well-balanced high-order centred schemes for non-conservative hyperbolic systems. Applications to shallow water equations with fixed and mobile bed, *Adv. Water Resour.*, *32*(6), 834–844.

Castro-Díaz, M. J., E. D. Fernández-Nieto, M. J. González-Vida, and C. Parés-Madroñal (2011), Numerical treatment of the loss of hyperbolicity of the two-layer shallow-water system, *J. Sci. Comput.*, *48*(1–3), 16–40.

Cordier, S., M. H. Le, and T. Morales de Luna (2011), Bedload transport in shallow water models: Why splitting (may) fail, how hyperbolicity (can) help, *Adv. Water Resour.*, *34*, 980–989.

Cui, Y., and G. Parker (2005), Numerical model of sediment pulses and supply disturbances in mountain rivers, *J. Hydraul. Eng.*, *131*(8), 646–656.

Dal Maso, G., P. Le Floch, and F. Murat (1995), Definition and weak stability of nonconservative products, *J. Math. Pures Appl.*, *74*(6), 483–548.

De Vries, M. (1965), Considerations about non-steady bed-load transport in open channels, paper presented at 11th Congress IAHR, Int. Assoc. for Hydraul. Res., Leningrad, Russia.
Di Silvio, G. (1992), Sediment exchange between stream and bottom: A four layer model, paper presented at the International Grain Sorting Seminar, Int. Assoc. for Hydraul. Res., Monte Verità, Ascona, Switzerland.
Dumbser, M., and E. F. Toro (2011), A simple extension of the Osher Riemann solver to non-conservative hyperbolic systems, *J. Sci. Comput.*, *48*(1–3), 70–88.
Egiazaroff, V. I. (1965), Calculation of non-uniform sediment concentrations, *J. Hydraul. Div. Am. Soc. Civ. Eng.*, *91*(4), 225–247.
Fasolato, G., P. Ronco, and G. Di Silvio (2009), How fast and how far do variable boundary conditions affect river morphodynamics?, *J. Hydraul. Res.*, *47*(3), 329339.
Furbish, D. J., J. C. Roseberry, and M. W. Schmeeckle (2012), A probabilistic description of the bed load sediment flux: 3. The particle velocity distribution and the diffusive flux, *J. Geophys. Res.*, *117*, F03033, doi:10.1029/2012JF002355.
Gray, J. M. N. T., and C. Ancey (2011), Multi-component particle-size segregation in shallow granular avalanches, *J. Fluid Mech.*, *678*, 535–588.
Hirano, M. (1971), River bed degradation with armoring, *Trans. Jpn. Soc. Civ. Eng.*, *3*, 194–195.
Hirano, M. (1972), Studies on variation and equilibrium state of a river bed composed of nonuniform material, *Trans. Jpn. Soc. Civ. Eng.*, *4*, 128–129.
Hoey, T. B., and R. I. Ferguson (1994), Numerical simulation of downstream fining by selective transport in gravel bed rivers: Model development and illustration, *Water Resour. Res.*, *30*, 2251–2260.
Holly, F. M., and J. L. Rahuel (1990), New numerical/physical framework for mobile-bed modelling, part I: Numerical and physical principles, *J. Hydraul. Res.*, *28*, 401–416.
Iseya, F., and H. Ikeda (1987), Pulsations in bedload transport rates induced by a longitudinal sediment sorting: A flume study using sand and gravel mixtures, *Geogr. Ann., Ser. A*, *69*(1), 15–27.
Kuhnle, R. A., and J. Southard (1988), Bed load transport fluctuations in a gravel bed laboratory channel, *Water Resour. Res.*, *24*, 247–260.
Lanzoni, S., and M. Tubino (1999), Grain sorting and bar instability, *J. Fluid Mech.*, *393*, 149–174.
Lanzoni, S., A. Siviglia, A. Frascati, and G. Seminara (2006), Long waves in erodible channels and morphodynamic influence, *Water Resour. Res.*, *42*, W06D17, doi:10.1029/2006WR004916.
Lyn, D. (1987), Unsteady sediment transport modeling, *J. Hydraul. Eng*, *113*(1), 1–15.
Lyn, D., and M. Altinakar (2002), St. Venant Exner equations for near-critical and transcritical flows, *J. Hydraul. Eng.*, *128*(6), 579–587.
Mazza de Almeida, G. A., and J. F. Rodríguez (2011), Understanding pool-riffle dynamics through continuous morphological simulations, *Water Resour. Res.*, *47*, W01502, doi:10.1029/2010WR009170.
Meyer-Peter, E., and R. Müller (1948), Formulas for bedload transport, paper presented at 2nd Meeting, Int. Assoc. of Hydraul. Eng. and Res., Stockholm.
Mosselman, E. (2012), Modelling sediment transport and morphodynamics of gravel-bed rivers, in *Gravel Bed Rivers: Processes, Tools, Environments*, pp. 101–115, John Wiley, Chichester, U. K.
Mosselman, E., K. Sloff, and S. van Vuren (2008), Different sediment mixtures at constant flow conditions can produce the same celerity of bed disturbances, paper presented at River Flow 2008: Proceedings of the International Conference on Fluvial Hydraulics, IAHR, Cesme, Izmir, Turkey.
Parés, C. (2006), Numerical methods for non-conservative hyperbolic systems: A theoretical framework, *SIAM J. Numer. Anal.*, *44*, 300–321.
Parker, G. (1990), Surface-based bedload transport relation for gravel rivers, *J. Hydraul. Res.*, *28*(4), 417–436.
Parker, G. (1991), Selective sorting and abrasion of river gravel. I. Theory, *J. Hydraul. Eng.*, *117*, 113–149.
Parker, G. (2004), *Ebook on 1D Sediment Transport Morphodynamics With Applications to Rivers and Turbidity Currents*. [Available at http://hydrolab.illinois.edu/people/parkerg/powerpoint_lectures.htm.]
Parker, G., and E. D. Andrews (1985), Sorting of bed load sediment by flow in meander bends, *Water Resour. Res.*, *21*(9), 1361–1373.
Parker, G., C. Paola, and S. Leclair (2000), Probabilistic Exner sediment continuity equation for mixtures with no active layer, *J. Hydraul. Eng.*, *126*, 818–826.
Recking, A., P. Frey, and P. Belleudy (2009), An experimental investigation of mechanisms involved in bed load sheet production and migration, *J. Geophys. Res.*, *114*, F03010, doi:10.1029/2008JF000990.
Ribberink, J. S. (1987), Mathematical modelling of one-dimensional morphological changes in rivers with non-uniform sediment, PhD thesis, Delft Univ. of Technol., Delft, Netherlands. [Available at http://repository.tudelft.nl/view/ir/uuid%3Abdfc1519-a71d-4752-83f7-3ebf1bb 890e9/.]
Seminara, G., M. Colombini, and G. Parker (1996), Nearly pure sorting waves and formation of bedload sheets, *J. Fluid Mech.*, *312*, 253–278.
Sieben, J. (1997), Modelling of hydraulics and morphology in mountain rivers, PhD thesis, Delft Univ. of Technol., Delft, Netherlands.
Sieben, J., and C. J. Sloff (1994), *Analysis of a 2DH Mathematical Model for Mountain Rivers With Graded Sediments, International Workshop on Floods and Inundations and Related to Large Earth Movements*, edited by A. Armanini, IAHS Publication, Trento, Italy.
Sloff, C. J., and E. Mosselman (2012), Bifurcation modelling in a meandering gravel-sand bed rivers, *Earth Surf. Processes Landforms*, *37*, 1556–1566.
Sloff, C. J., H. R. A. Jagers, Y. Kitamura, and P. Kitamura (2001), 2D morphodynamic modelling with graded sediment, paper presented at the 2nd Symposium on River, Coastal and Estuarine Morphodynamics, Int. Assoc. for Hydraul. Res., Obihiro, Japan.
Suzuki, K. (1976), On the propagation of a disturbance on the bed composition of an open channel, Technical Report, *R 1976 /09/L*, Delft Univ. of Technol., Delft, Netherlands.
Toro, E. F. (2001), *Shock-Capturing Methods for Free-Surface Shallow Flows*, John Wiley, Chichester, U. K.
Toro, E. F. (2009), *Riemann Solvers and Numerical Methods for Fluid Dynamics: A Practical Introduction*, Springer, Heidelberg.
Toro-Escobar, C. M., G. Parker, and C. Paola (1996), Transfer function for the deposition of poorly sorted gravel in response to streambed aggradation, *J. Hydraul. Res.*, *34*(16), 35–53.
Vetsch, D., D. Ehrbar, S. Peter, P. Russelot, C. Volz, L. Vonwiller, R. Faeh, D. Farshi, R. Mueller, and R. Veprek (2006–2013), BASEMENT—Basic Simulation Environment for Computation of Environmental Flow and Natural Hazard Simulation, in *Software Manual*, Laboratory of Hydraulics, Hydrology and Glaciology (VAW), ETH Zurich, Switzerland. [Available at www.basement.ethz.ch.]
Viparelli, E., O. E. Sequeiros, A. Cantelli, P. R. Wilcock, and G. Parker (2010), River morphodynamics with creation/consumption of grain size stratigraphy 2: Numerical model, *J. Hydraul. Res.*, *46*(6), 726–741.
Wilcock, P. R., and J. Crowe (2003), Surface-based transport model for mixed-size sediment, *J. Hydraul. Eng.*, *129*(2), 120–128.